

✉ Universität Bremen | MARUM | 28359 Bremen

**To**

**Gerald (Jerry) Dickens**

***Editor of *Climate of the Past****

Dr.

**Thomas Westerhold**

Research Scientist

Leobener Strasse  
MARUM building, Room 0220  
28359 Bremen – Germany

Telefon +49 421 218 – 65 672  
E-Mail [twesterhold@marum.de](mailto:twesterhold@marum.de)  
www [www.marum.de](http://www.marum.de)

**Letter to the editor – Authors' response**

15. August 2015

Dear Jerry,

Herewith we submit our revised manuscript entitled: “Astronomical Calibration of the Geological Timescale: Closing the Middle Eocene Gap”.

We thank you and the referees for your time and effort to evaluate our manuscript. We appreciate the comments and constructive criticism of both referees that encouraged us to carefully revise the manuscript accordingly.

Please find below a point-by-point reply to the comments of the referees and editor (original comments are given in italics).

The manuscript benefited from the criticism of Referee #1 and #2 regarding the lack of a comparison between the terrestrial and deep-sea calibrated Geomagnetic Polarity Time Scale (GPTS). In order to address these concerns, we (i) included a fully new section in the discussion of the manuscript, and (ii) modified Figure 7 by adding the two most recent terrestrial calibrations and the calibration tie-points used. We also modified tables accordingly and added a new table to the Supplementary (S13) to document the uncertainty in duration of magnetochrons due to the error in the stacked deep-sea magnetic anomaly profile of Cande & Kent 1992 used for GPTS calibration. For the final submission we have moved tables S4 to S13 to the supplement and put a link to the Pangaea database for extensive tables S1-3. We are confident that our stratigraphy for Site 702 and 1263 is consistent and robust and an important step towards a new and accurate calibration of the GPTS.

We hope that our revised manuscript meets the requirements to be published in *Climate of the Past*.

Sincerely,

Thomas Westerhold, Ursula Röhl, Thomas Frederichs, Steven M. Bohaty, James C. Zachos

## Point-by-point reply to the comments

### Reply to comments by Editor Gerald (Jerry) Dickens

---

*My major comment comes as a triple whammy. Look carefully at Figure 5. It does not make sense, especially without discussion. First, the y-axis in panel A ( $d_{13}C$ ) should be reversed, so as to conform to previous figures and most literature. Far more crucially, the  $d_{13}C$  records at Sites 702 and 1263 do not align. There are only three options: the stratigraphy at one or both sites is incorrect (which is not good for a paper mostly on stratigraphy), the  $d_{13}C$  of surface waters in the south Atlantic during the middle Eocene diverged (which would be really interesting and worthy of comment), or the  $d_{13}C$  of bulk sediment is not recording a primary signal (which then places serious doubts on the use of the records for tuning age models). This problem has to be addressed in a revised manuscript.*

Response to whammy 1: *The y-axis in panel A ( $d_{13}C$ ) should be reversed, so as to conform to previous figures and most literature.*

We plotted  $\delta^{13}C$  data in Figure 5 on a reversed axis to improve easier visibility of the correlation to eccentricity solution data. Alternatively, we could reverse the axis as suggested, but then we would need to also reverse the eccentricity axis to show the extraordinary similarity of amplitude modulation in the eccentricity and  $\delta^{13}C$  data. It is not uncommon to plot the  $\delta^{13}C$  axis this way (see Pälike et al. 2006 – Science ;Zachos et al. 2010 - EPSL, Kirtland-Turner et al. 2014 - Nature Geoscience). For analysis/interpretation of the data we would like to keep the axis this way. In the initial presentation of the datasets (Fig. 2), the  $\delta^{13}C$  data are plotted conventionally with the more positive values upwards.

Response to whammy 2: *Far more crucially, the  $d_{13}C$  records at Sites 702 and 1263 do not align. There are only three options: the stratigraphy at one or both sites is incorrect (which is not good for a paper mostly on stratigraphy)...*

Given all the factors (variables) that influence seawater carbon isotopes and carbonate production and deposition, there's no a priori reason to assume that bulk sediment  $\delta^{13}C$  should co-vary in records across the ocean basins, and yet they often do, and so we use these patterns for chemostratigraphy. However, the fact that the mean  $\delta^{13}C$  values deviate between sites on long time scales should not come as surprise, especially as ocean circulation and biology is shifting. The challenge for stratigraphic applications is to be able to extract the orbital patterns from these records, the relative modulation of which should be similar, even as the means deviate. The Oligocene-Miocene is good example where the 405-kyr cycles can be extracted and correlated even as mean values deviate between records.

The  $\delta^{13}C$  records in our study do align between 41.5 and 44.5 Ma with similar absolute  $\delta^{13}C$  values and similar trends/orbital-scale cyclicity. Between 44.5 and 47 Ma Site 702 is offset relative to Site 1263 by 0.3-0.4‰ (Figure 5 of the manuscript) but trends and pattern of orbitally-paced events are similar. In the interval 47 to 49 Ma offset values and trends are different, but the pattern at ~48 Ma is the same (double  $\delta^{13}C$  excursion).

The 405-kyr eccentricity cyclostratigraphy of both sites is consistent as in Figure 5 b and c of the submitted manuscript. Despite the offset from 44.5 to 49 Ma both  $\delta^{13}C$  curves show a very similar pattern from 45.5 to 47 Ma including the minimum in amplitude modulation at eccentricity 405-kyr cycle 113. In Figure 1, we plot both data on the same  $\delta^{13}C$  axis and on separate  $\delta^{13}C$  axis to demonstrate the coherently corresponding pattern of both records. This clearly suggests that the stratigraphy between sites is consistent and correct. The offset from 44.5 to 48 Ma is making the visual comparison a bit more difficult. We address this offset in the next response (below).

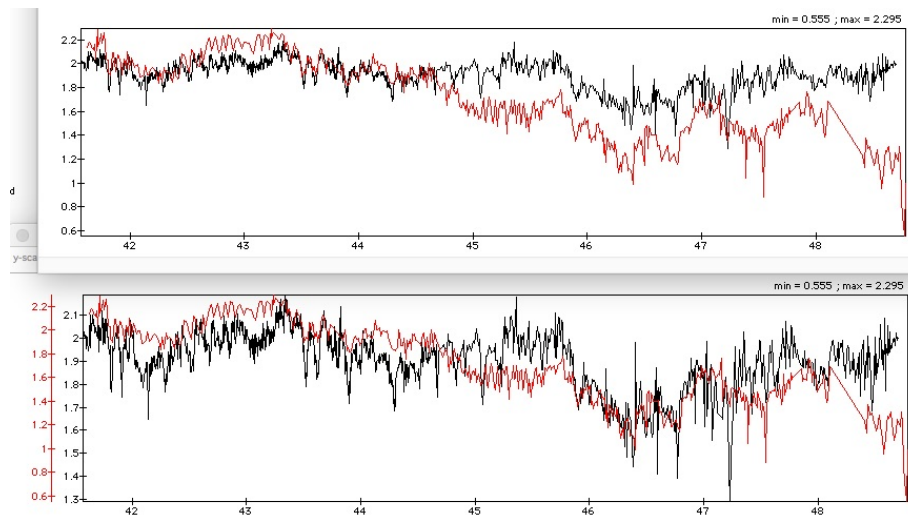


**Figure 1.**  $\delta^{13}\text{C}$  bulk data from 702B (red) and 1263 (black) plotted on the tuned age model. Top panel shows both records plotted on the same  $\delta^{13}\text{C}$  axis. Lower panel shows both records plotted on separate  $\delta^{13}\text{C}$  axis. The upper panel shows the overall good correlation between the data from 42 to 44.5 Ma, the lower panel shows the very good correlation between 45 to 47 Ma, and around 48 Ma. Therefore, we think that the stratigraphy at both sites is correct back to 48 Ma.

The problematic interval is between 47 and 48 Ma, where the bulk isotope data have offset values and trends. The two peaks in 702B  $\delta^{13}\text{C}$  data 47.35 (~179 mbsf) and 47.5 Ma (~182 mbsf, see Figure 2) are single points and therefore should not be over interpreted as  $\delta^{13}\text{C}$  excursion or used for direct correlation to 1263. The  $\delta^{13}\text{C}$  excursion seen in 1263 at 47.2 Ma is not present in 702B bulk data but can be seen in unpublished XRF core scanning Fe/Ca intensity data (~176.5 mbsf) as a significant peak indicating dissolution of carbonate. We are currently developing a high-resolution benthic isotope record to explore this interval in both 702B and 1263 to re-evaluate the tuning. The cyclostratigraphy for 1263 in this interval is straightforward because the 405-kyr cycles can be clearly identified (see Figure 5 in the manuscript, cycles 14-16). 405-kyr cycles 14 and 15 are hard to recognize in 702B (see Figure 5 in the manuscript), but cycle 16 can be identified and also matches cycle 16 in 1263 with the prominent double  $\delta^{13}\text{C}$  peaks at 48.0 and 48.1 Ma. Cycle 16 in both record is located in C21r and thus we are confident that there is no major gap in 702B.

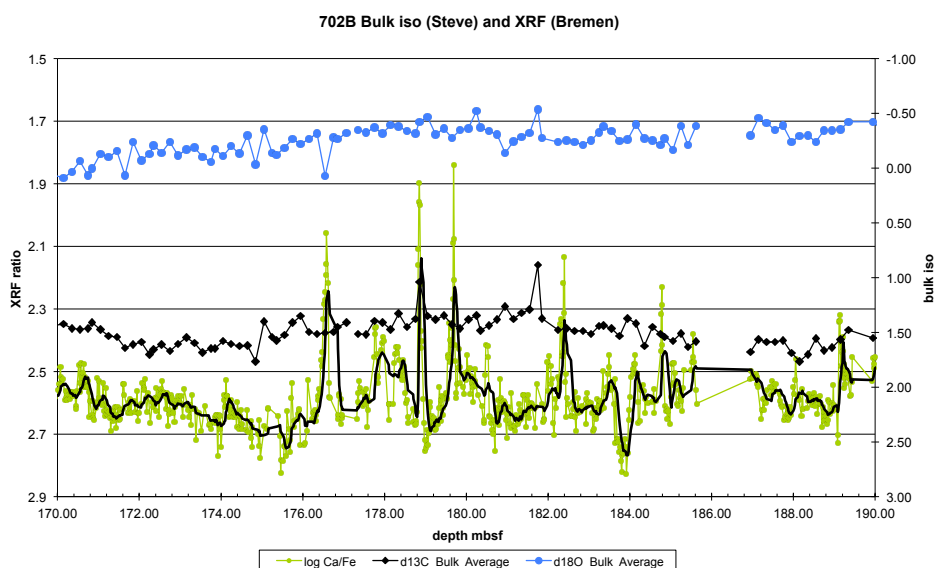


**Figure 2.**  $\delta^{13}\text{C}$  (black) and  $\delta^{18}\text{O}$  (blue) bulk data from 702B plotted with unpublished XRF core scanning Fe/Ca data (light green – 2cm resolution; dark green – 9pt. average).

Response to whammy 3: ..., the  $\delta^{13}\text{C}$  of surface waters in the south Atlantic during the middle Eocene diverged (which would be really interesting and worthy of comment), ... or the  $\delta^{13}\text{C}$  of bulk sediment is not recording a primary signal (which then places serious doubts on the use of the records for tuning age models).

Because the stratigraphy is consistent between Sites 702 and 1263, the offset in the  $\delta^{13}\text{C}$  signal could be a result of changes in the surface water at Site 702. One site is from the middle of the South Atlantic gyre (1263) and the other site is at higher latitude on the edge of the gyre (702). Maybe there were differences in surface-water nutrient levels or/and stratification. Even though both sites are comprised of slowly accumulated pelagic carbonates, Site 702 would likely have been subject to higher nutrient conditions and/or more variability in nutrient supply. There is a bit of biogenic silica (radiolarians & silicoflagellates) in the upper middle Eocene section of Site 702. The lower bulk  $\delta^{13}\text{C}$  values in the older part of the record at Site 702 could be indicative of higher nutrient levels or a deeper depth of production of calcareous nannoplankton. Given all the variables that control mixed-layer  $\delta^{13}\text{C}$ -DIC (including also air-sea  $\text{CO}_2$  exchange) the two sites shouldn't really be expected to have similar bulk  $\delta^{13}\text{C}$  values.

No benthic  $\delta^{13}\text{C}$  data are published from this interval from Site 1263 (this is one focus of our ongoing studies). Very low-resolution benthic  $\delta^{13}\text{C}$  data are available for Hole 702B from Katz & Miller (1991) showing a possible 0.2‰ shift in benthic data at 44.5 Ma (Figure 3). This might suggest changes in surface and deep ocean carbon signatures, but, due to the rather low resolution and lack of data from Site 1263, all of this is currently speculative and needs to be validated by high-resolution benthic isotope data from both Sites 702 and 1263. Looking at the very similar patterns in Figure 1 between the  $\delta^{13}\text{C}$  bulk data we think that both sites are recording the primary signal and it is very unlikely that diagenesis has altered the  $\delta^{13}\text{C}$  signal at both sites the same way. The shift in  $\delta^{13}\text{C}$  bulk data at 44.5 Ma does not influence the stratigraphy and thus the results of the submitted manuscript. We will investigate this very interesting feature in a follow up study that focuses on paleoceanographic interpretations.

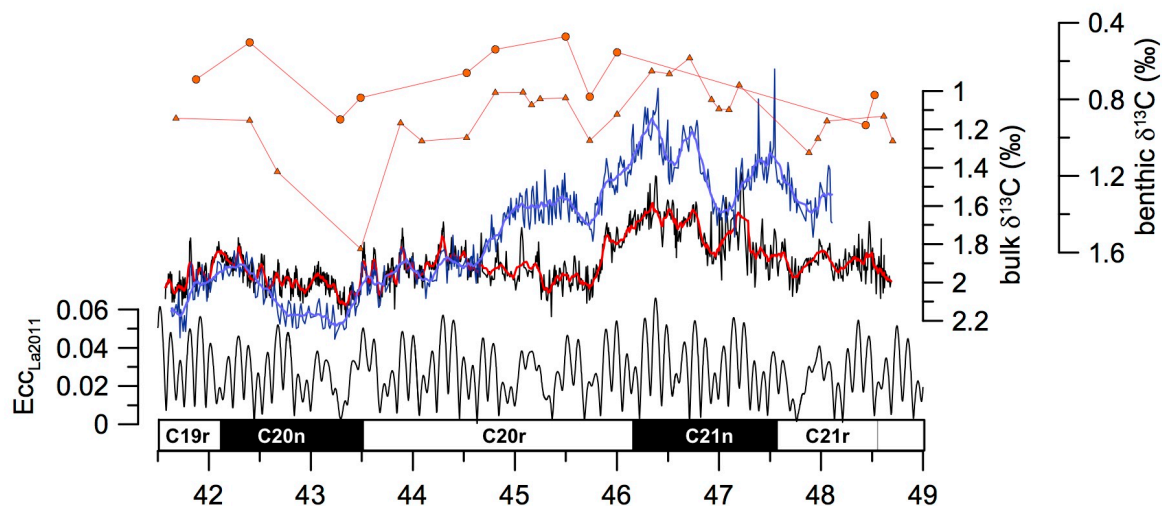


**Figure 3.** modified from figure 5a of the submitted manuscript. Middle Eocene South Atlantic bulk and benthic stable carbon isotope data, the La2011 orbital eccentricity (Laskar et al. 2011), and magnetostratigraphy from 41.5 to 49.5 Ma on a common astronomical calibrated age model. Data from ODP Sites: 702B bulk (blue, this study) and benthic (*N. truempyi* - dots and *Cibicidoides* spp. - triangles, (Katz & Miller 1991)) from Islas Orcadas Rise, 1263 bulk (black, this study). The thick blue (702B) and red (1263) lines are 11 point running averages.

*I offer a few additional comments.*

-- Page 1666 --

*Line 2: Needs rewording and comma "... reconstructions, high accuracy ..."*

*Lines 3-5: Rewrite as the word accuracy becomes redundant and superfluous here.*

We reworded the first lines of the Abstract to state: "To explore causes and consequences of past climate change, very accurate age models such as those provided by the Astronomical Time Scale (ATS) are needed. Beyond 40 million years the accuracy of the ATS critically depends on the correctness of orbital models and radio-isotopic dating techniques."

*Line 23 (and throughout): Avoid Latin abbreviations (such as "e.g.") in the middle of text. This is sloppy writing.*

We deleted "e.g." in the entire text.

-- Page 1679 --

*Lines 21-24: This sentence is unintelligible to me, and although I can be quite stupid at times, I will suspect the same for many readers. I would add 1-2 sentences, so that these concepts are clearly explained to everyone.*

We added several more sentences to the manuscript to reveal why it is important to find the transition from libration to circulation. A good description of the problem is given by Pälike et al. (2004), which is cited in the text.

-- Page 1680 --

*Should be "... is the key to exploring ..."*

We corrected this in the revised manuscript.

---

### **Reply to the comments by an anonymous Referee #1 and Referee #2 (James Ogg)**

An in-depth reply to both reviewers is given in the reply to the interactive comments on the Climate of the Past interactive discussion (<http://www.clim-past-discuss.net/11/C900/2015/cpd-11-C900-2015.pdf>).

As proposed in the comment to anonymous Referee #1 we have added a new section in the discussion on the comparison of the early to middle Eocene GPTS calibration between terrestrial and deep-sea GPTS. We have modified Figure 7A accordingly.

Regarding the comments/suggestions by Referee #2 (James Ogg):

- (1) - J. Ogg asked for separate zoom in figure(s) for Sites 702 and 1263 data to show possible expression of precession and short-eccentricity cycles on core images in some intervals. We have added a short discussion of these points and a new Figure S4 to the supplementary information to address this suggestion.
- (2) - J. Ogg asked to add one or two sentences that would summarize the cause-effect of why long-term eccentricity envelopes on climate cycles would affect the carbon-isotope composition of marine plankton. We added the following to the supplement of the revised manuscript: "The strong 405-kyr cycle in benthic and bulk  $\delta^{13}\text{C}$  data as well as simulated  $\delta^{13}\text{C}$  results from a resonance associated with the long residence time of carbon in the ocean (Broecker and Peng, 1982; Pälike et al., 2006a; Ma et al., 2011). Periodic changes in oceanic  $\delta^{13}\text{C}$  on Milankovitch time scales are likely caused by changes in weathering induced carbon input changing the burial ratio of  $\text{CaCO}_3$  to organic carbon (Cramer et al., 2003; Ma et al., 2011). An increase in weathering intensity and riverine carbon supply will increase the burial ratio of  $\text{CaCO}_3$  to organic carbon leading to a decrease in  $\delta^{13}\text{C}$  (minima, lighter values in bulk  $\delta^{13}\text{C}$ ). During eccentricity maxima weathering intensity and nutrient supply is enhanced leading via the biosphere productivity feedback to lighter bulk  $\delta^{13}\text{C}$  values in the stable carbon isotope records."

(3) – J. Ogg suggested tuning the records to the short eccentricity cycle (100kyr). Our approach is to only apply minimal tuning of the records. Adding more tuning tie points could be done, but would already introduce much more characteristics of the target curve into the record. At the same time the improvements on absolute ages on magnetostratigraphic chrons or subchrons will be minimal. For the revised manuscript we suggest not to increase the number of tie points. The extra level of tuning mentioned by J. Ogg is best done once high-resolution benthic records are developed

(4) – J. Ogg asked to mark a set of selected or averaged ages for magnetochrons and datums, plus the uncertainty in bold as a “best estimate” that can be used to make a reference time scale for polarity chrons, spreading rates, microfossil datums, etc.. In Table 1 of the manuscript we have marked the selected datums in bold.

– J. Ogg also asked to include an enlarged vertical-scale timescale figure showing chrons, climate events with perhaps a generalized carbon-isotope curve, microfossil events and the interpreted/labelled 405-kyr cycles plotted against a numerical time scale for the interval of chrons C22-C18. At first thought this seems to be a very good idea, however, at second thought we decided not to make such a figure for several reasons: a reference carbon isotope curve is desirable for Chron C18 to C22 but still not complete. In ongoing studies we will fill the Chron C18 interval with high resolution bulk isotope data and combine these with published records for the Middle Eocene Climate Optimum (MECO) interval. The MECO stratigraphy is currently revised by a group at NOC (UK, Steve Bohaty and coworkers). Therefore, a complete carbon isotope curve is not available at the moment. It will be the focus of later manuscripts to compile the entire stratigraphy of the middle Eocene. Defining the positions and ages for microfossil events is very important. Ongoing efforts are focused on Site 1263 records with C. Agnini (Padova) and I. Raffi (Chieti) to refine the calcareous nannofossil biostratigraphy. We think at this stage it would not be very helpful to provide a table with bioevents as they will be revised soon anyway. Once both the carbon isotope stratigraphy and revised nannofossil datums are available we will compile a bio-magneto-chemo-cyclostratigraphy for the middle Eocene and then will be able to compile a figure like envisaged by J. Ogg.

– J. Ogg suggested for stratigraphic placement of events within chrons, such as microfossil datums, to use percent-from-base, rather than percent-from-top, because one usually goes forward in geologic time. We changed this in the manuscript accordingly, see Table S5.

– J. Ogg suggested using basal ages for reversed-polarity chrons, rather than tabulating these as top-ages of the underlying/preceding normal-polarity chrons. We refrain from doing so because it is more personal preference. The current scheme is consistent with many other manuscripts published by our team already (see Westerhold et al. 2014 in *Climate of the Past* table 1; *Clim. Past*, 10, 955–973, 2014; doi:10.5194/cp-10-955-2014).

– J. Ogg suggested including uncertainties for the CK95 (derived from their supplement table on uncertainties on anomaly widths; which is partly included in GTS2012 Table 5.2) in the comparison table of chron durations. We have now added a new table to the supplementary dataset (Table S13) with the minimum and maximum durations for CK95, GPTS2004, and GPTS2012; these durations are based on the error given for the mean width of magnetic anomalies as published in Table 4 of Cande & Kent (1992) compared to the duration estimate from this manuscript. We have included this in the discussion of the manuscript. This table shows the rather large uncertainty around C22 and C23 also in the deep-sea anomaly width definition by Cande and Kent (1992). Based on their Table 4 C21r, C22r and C23 have an error in the anomaly width of 12 to 17%, which can also help to explain larger differences in durations between the terrestrial and deep-sea records. A deep-sea biomagneto-cyclostratigraphic record is needed to test ODP Site 1258 results in order to evaluate the true duration of magnetochrons C22 and C23.

– J. Ogg suggested that we include remarks on why some cycle-derived durations are significantly longer, but others are significantly shorter, in a non-systematic pattern compared to CK95 (therefore also the spline-fit GTS2012 that used CK95 anomaly widths). We added a few sentences to the discussion to address this point in the Section 5.1 'Consistent absolute ages for the Paleogene.'

Please find the marked changes to the main text below

# Astronomical Calibration of the Geological Timescale: Closing the Middle Eocene Gap

Thomas Westerhold<sup>1</sup>, Ursula Röhl<sup>1</sup>, Thomas Frederichs<sup>2</sup>, Steven M. Bohaty<sup>3</sup>, James C. Zachos<sup>4</sup>

[1]MARUM – Center for Marine Environmental Sciences, University of Bremen, Leobener Strasse, 28359 Bremen, Germany

[2]Department of Geosciences, University of Bremen, 28359 Bremen, Germany

[3]Ocean and Earth Science, University of Southampton, National Oceanography Centre, Southampton, SO14 3ZH, UK

[4]University of California, Santa Cruz, California, USA

Correspondence to: twesterhold@marum.de, phone ++4942121865672

## Abstract

To explore cause and consequences of past climate change, very accurate, age models such as those provided by the Astronomical Time Scale (ATS) are needed. Beyond 40 million years the accuracy of the ATS critically depends on the correctness of orbital models and radio-isotopic dating techniques. Discrepancies in the age dating of sedimentary successions and the lack of suitable records spanning the middle Eocene have prevented development of a continuous astronomically calibrated geological timescale for the entire Cenozoic Era. We now solve this problem by constructing an independent astrochronological stratigraphy based on Earth's stable 405-kyr eccentricity cycle between 41 and 48 million years ago (Ma) with new data from deep-sea sedimentary sequences in the South Atlantic Ocean. This new link completes the Paleogene astronomical time scale and confirms the intercalibration of radio-isotopic and astronomical dating methods back through the Paleocene-Eocene Thermal Maximum (PETM, 55.930 Ma) and the Cretaceous/Paleogene boundary (66.022 Ma). Coupling of the Paleogene 405-kyr cyclostratigraphic frameworks across the middle Eocene further paves the way for extending the ATS into the Mesozoic.

Autor  
Gelöscht: reconstructions highly

Autor  
Gelöscht: accurac

Autor  
Gelöscht: y

Autor  
Gelöscht: inevitable

Autor  
Gelöscht: The highly accurate astronomical calibration of the geological time scale b

Autor  
Gelöscht: accuracy of

Autor  
Gelöscht: Astronomical Time Scale (

Autor  
Gelöscht: )

## 40 1. Introduction

41 Accurate absolute age determinations are essential for the geologic study of Earth history.  
42 In recent decades the age calibration of the Geological Time Scale was revolutionized by  
43 the discovery of astronomically driven cycles in both terrestrial and marine sedimentary  
44 archives (Hilgen, 2010). Development of cyclostratigraphic records and application of  
45 astronomical tuning (Hinnov, 2013) have evolved into powerful chronostratigraphic tools  
46 for highly accurate calibration of the Neogene time scale (Lourens et al., 2004), as well as  
47 synchronizing the widely used radio-isotopic  $^{40}\text{Ar}/^{39}\text{Ar}$  and U/Pb absolute dating methods  
48 (Kuiper et al., 2008). Limits in the accuracy of astronomically calibrated geological time  
49 scale (ATS) are a consequence of uncertainties in astronomical solutions (Laskar et al.,  
50 2011a; Laskar et al., 2011b; Laskar et al., 2004). Earth's orbital eccentricity, the deviation  
51 of Earth's orbit around the sun from a perfect cycle, is widely used for astronomical  
52 calibrations (Hilgen, 2010; Hinnov, 2013). Accurate calculations of Earth's short  
53 eccentricity cycle, which has an average period of ~100-kyr, are currently reliable back to  
54 50 Ma and most likely will never extend beyond 60 Ma (Laskar et al., 2011b; Westerhold  
55 et al., 2012) due to chaotic behavior of large bodies within the asteroid belt. Despite this,  
56 the long (405-kyr) eccentricity cycle is stable back to 200 Ma and thus serves as a  
57 metronome for basic cyclostratigraphic calibration of time series (Hinnov and Hilgen,  
58 2012; Laskar et al., 2004) in Mesozoic and early Cenozoic time. Beyond the 50 Ma limit  
59 for short eccentricity multimillion-year-long geological records (Hinnov and Hilgen,  
60 2012) with a 405-kyr eccentricity cyclostratigraphic framework have to be anchored in  
61 absolute time (Kuiper et al., 2008) by very precise radio-isotopic ages from ash layers.

62 Because controversy exists regarding the accuracy of high-precision radio-isotope dating  
63 and astrochronological calibrations in the Paleocene and Eocene (Kuiper et al., 2008;  
64 Westerhold et al., 2012) and the exact age of the Fish Canyon Tuff (FCT) standard for  
65  $^{40}\text{Ar}/^{39}\text{Ar}$  dating (Kuiper et al., 2008; Westerhold et al., 2012; Channell et al., 2010;  
66 Phillips and Matchan, 2013; Renne et al., 2010; Renne et al., 1998; Rivera et al., 2011;  
67 Wotzlaw et al., 2014; Wotzlaw et al., 2013; Zeeden et al., 2014), extension of the highly  
68 accurate ATS beyond 50 Ma into the early Cenozoic and Mesozoic time is not possible.  
69 What is needed is a calibration of the Geological Time Scale in the Eocene and Paleocene  
70 that is independent from radio-isotopic dating uncertainties and unstable components of

Autor

Gelöscht: , e.g.,

72 astronomical solutions. The best approach is to establish a complete stratigraphic  
73 framework for the Cenozoic that is based on the identification of the stable 405-kyr  
74 eccentricity cycle and is rooted in the Neogene to late Eocene where all components of  
75 the orbital solutions are stable and uncertainties in radio-isotopic ages are negligible. The  
76 complete stratigraphic framework will show which published absolute ages within the  
77 Eocene and Paleocene epochs, particularly the ages of the Paleocene/Eocene (Westerhold  
78 et al., 2012; Charles et al., 2011; Hilgen et al., 2010; Westerhold et al., 2007; Westerhold  
79 et al., 2009) and Cretaceous/Paleogene boundaries (Kuiper et al., 2008; Hilgen et al.,  
80 2010; Dinarès-Turell et al., 2014; Hilgen et al., 2015; Renne et al., 2013; Westerhold et  
81 al., 2008), are correct and consistent with radio-isotopic ages (Kuiper et al., 2008; Renne  
82 et al., 2013; Renne et al., 1998; Rivera et al., 2011). To date, a complete stratigraphic  
83 framework has not been possible due to the lack of well-defined cyclostratigraphic  
84 records spanning the middle Eocene (Pälike and Hilgen, 2008).

85 Herein, we close the middle Eocene gap in orbitally tuned datasets (Aubry, 1995; Pälike  
86 and Hilgen, 2008) by developing an integrated stratigraphic framework based on the  
87 identification of the stable 405-kyr cycle (Hinnov and Hilgen, 2012) between 41 and 48  
88 Ma using new data from Ocean Drilling Program (ODP) Sites 702 (Leg 114, (Shipboard  
89 Scientific Party, 1988)) and 1263 (Leg 208, (Shipboard Scientific Party, 2004)) in the  
90 South Atlantic Ocean (Fig. 1). This was achieved by establishing a magnetostratigraphy  
91 across magnetic polarity chrons C20r and C21n at Site 1263, then combining this with  
92 high-resolution bulk carbon isotope ( $\delta^{13}\text{C}$ ) records from Sites 702 and 1263. These new  
93 data, together with previously available shipboard stratigraphic data allow us to construct  
94 a robust 405-kyr cyclostratigraphic framework across a ~7-Myr window of the middle  
95 Eocene.

96

## 97 **2. Material and methods**

### 98 **2.1 Study sites**

99 For this study we generated new geochemical and paleomagnetic data on carbonate rich  
100 sediments from Ocean Drilling Program (ODP) South Atlantic Site 702 (Leg 114,  
101 (Shipboard Scientific Party, 1988)) and Site 1263 (Leg 208, (Shipboard Scientific Party,

102 2004)) (Fig. 1). ODP Site 702 is located in the southwestern South Atlantic on the central  
103 part of the Islas Orcadas Rise (50°56.79'S, 26°22.12'W) in 3083.4 m water depth. In April  
104 1987 only a single hole (Hole 702B) was drilled into Paleogene strata with extended core  
105 barrel (XCB) down to 294.3 meters below sea floor (mbsf), recovering a thick sequence  
106 of nannofossil ooze and chalk middle Eocene in age (Shipboard Scientific Party, 1988).  
107 For this study, samples were analyzed from Hole 702B in the ~90 and 210 mbsf **interval**  
108 (Fig. 2). ODP Site 1263 is located in the southeastern South Atlantic on Walvis Ridge  
109 (28°31.97'S, 2°46.77'E) in 2717 m water depth (Shipboard Scientific Party, 2004). At this  
110 site, a sequence of Paleogene strata was cored in four adjacent holes that have been  
111 combined to a composite record down to 340 meters composite depth (mcd). After  
112 revision of the Site 1263 composite record (see below), samples for this study were  
113 obtained from the interval between ~150 and 230 revised meters composite depth (rmcd)  
114 of 1263 (Fig. 2).

115

## 116 **2.2 Bulk stable isotope data**

117 Bulk carbonate  $\delta^{13}\text{C}$  measurements were made in two different labs on freeze-dried and  
118 pulverized sediment samples from ODP Sites 702 and 1263. A total of 539 samples from  
119 Site 702 were analyzed at University of California Santa Cruz (UCSC) between Sections  
120 702B-11X-1 and 702B-22X-CC at an average sampling resolution of 20 cm (~13 kyr  
121 temporal resolution, Table S1, Fig. 2). A total of 1157 samples in total were analyzed  
122 from Site 1263 (Table S2, Fig. 2). 668 of these samples spanning mid magnetochron  
123 C19r to mid C20r were **analyzed** at MARUM, University of Bremen, with an average  
124 resolution of 4 cm (5 kyr). The remaining 489 samples from Site 1263 spanning mid  
125 C20r to base C21r were measured at UCSC with average resolution of 10 cm (10 kyr).  
126 All  $\delta^{13}\text{C}$  data are reported relative to the Vienna Pee Dee Belemnite (VPDB) international  
127 standard, determined via adjustment to calibrated in-house standards and NBS-19.  
128 Analyses at MARUM were carried out on a Finnigan MAT 251 mass spectrometer  
129 equipped with an automated carbonate preparation line (Kiel I). The carbonate was  
130 reacted with orthophosphoric acid at 75 °C. Analytical precision based on replicate  
131 analyses of in-house standard (Solnhofen Limestone) averages 0.04‰ (1 $\sigma$ ) for  $\delta^{13}\text{C}$ .  
132 Stable isotope analyses at UCSC were performed on VG Prism and Optima dual-inlet

Autor

Gelöscht: section between

Autor

Gelöscht: processed

135 mass spectrometers coupled with Autocarb automated preparation devices in which the  
136 samples are reacted using a carousel device and common acid bath maintained at 90 °C.  
137 Analytical precision based on replicate analyses of an in-house Carrara Marble standard  
138 and NBS-19 averaged 0.05‰ (1σ) for δ<sup>13</sup>C.

139

### 140 **2.3 Paleomagnetic data Site 1263**

141 We measured natural remanent magnetization (NRM) on 100 discrete cube samples  
142 (gauge 2cm×2cm×2cm) to document magnetic polarity boundaries C19r to C21r at ODP  
143 Site 1263. Discrete samples were analyzed at the Department of Geosciences, University  
144 of Bremen. Paleomagnetic directions and magnetization intensities were measured on a  
145 cryogenic magnetometer (model 2G Enterprises 755 HR). NRM was measured on each  
146 sample before these were subjected to a systematic alternating field demagnetization  
147 treatment involving steps of 7.5, 10, 15, 20, 25, 30, 40 and 60 mT. Intensities of  
148 orthogonal magnetic components of the remanent magnetization were measured after  
149 each step. Raw inclination, declination, and intensity data for each measurement step is  
150 provided in Table S3, and the magnetostratigraphic interpretations are recorded in Table  
151 S4.

152

### 153 **2.4 Time series analysis**

154 To investigate Milankovitch-paced cyclicity in our datasets, we calculated evolutionary  
155 spectra in the depth and time domain to identify the dominant cycle periods and to detect  
156 distinct changes in these cycle periods. In order to obtain a first-order age model  
157 unaffected by astronomical tuning, we applied the magnetostratigraphy available for Sites  
158 702 (Clement and Hailwood, 1991) and 1263 (this study, Table S3) using the  
159 Geomagnetic Polarity Time Scale of (Cande and Kent, 1995). Wavelet analysis was used  
160 to compute evolutionary spectra using software provided by C. Torrence and G. Compo  
161 (available online at <http://paos.colorado.edu/research/wavelets>). Prior to wavelet analysis  
162 the data were detrended and normalized. Multitaper Method (MTM) spectra were then  
163 calculated with the SSA-MTM Toolkit (Ghil et al., 2002) using 3 tapers and resolution of  
164 2. Background estimate and confidence levels (90%, 95%, and 99%) are based on robust  
165 red noise estimation (Mann and Lees, 1996). Prior to analysis outliers and the long-term

166 trend were removed, and the time series was linearly resampled at 4-kyr (Site 702) and 2-  
167 kyr (Site 1263) intervals. After identification of the frequency and period of the short and  
168 long eccentricity-related cycles in the bulk  $\delta^{13}\text{C}$  data of both study sites, the 405-kyr  
169 cycle was extracted by band-pass filtering.

170

171

### 172 **3. Results**

173 All data are available online at <http://doi.pangaea.de/10.1594/PANGAEA.845986>.

174

#### 175 **3.1 Revised composite record for ODP Site 1263**

176 In order to ensure a fully complete stratigraphic record at Site 1263 we checked the  
177 shipboard composite record using shipboard magnetic susceptibility data and digital line  
178 scan high-resolution core images (Fig. S1). Small changes in the order of cm to a few dm  
179 were applied to optimize the splice and avoid coring induced disturbance in the isotope  
180 data. A major change had to be made around 120 rmc d which was reported as  
181 problematic during shipboard analysis (Shipboard Scientific Party, 2004). Core 1263C-  
182 2H was moved downwards by 2.52 m to match the base of Core 1263B-6H. Core 1263B-  
183 7H was then re-correlated to Core 1263C-7H by moving the core 3.34 m downward.  
184 Although this tie is difficult due to core disturbance the core images provided a good  
185 reference. This tie does not affect the record presented in this study because it is located  
186 at 125 rmc d and will be re-evaluated by additional bulk isotope data in the future. The  
187 composite splice was revised here down to 229.22 rmc d. Below this level, there is strong  
188 drilling disturbance across a 3–4-m interval. For completeness we report the full  
189 composite splice and offsets applied to adjust each core for Site 1263 in Table S7 and S8.

190

#### 191 **3.2 Magnetostratigraphic results and interpretation**

192 A detailed vector analysis according to the method by Kirschvink (Kirschvink, 1980)  
193 without anchoring to the origin of the orthogonal projections was applied to the results of  
194 the AF demagnetization of NRM to determine the characteristic remanent magnetization

195 (ChRM). Additionally the maximum angular deviation (MAD) values were computed  
196 reflecting the quality of individual magnetic component directions. MAD values are all  
197 below 10 degree (Figure 3).

198 Figures 3b and 3c display the demagnetization characteristics of a sample with reversed  
199 polarity from C19r and a sample with normal polarity from C21n, respectively. As an  
200 example for samples with demagnetization behavior with larger scatter (larger MAD),  
201 data from a sample within C21r is plotted in Figure 3d. The larger MADs that a few  
202 samples show are not simply related to the intensity of their remanent magnetization as  
203 can be seen from the data shown in Figure 3. The median destructive field (MDF) of the  
204 NRM demagnetization is comparable low for most of the samples. It ranges from 4 to 24  
205 mT (mean 7.1 +/- 4.1 mT) indicating a magnetically soft overprint in many samples. The  
206 interpretation of the ChRM in terms of magnetic polarity is focused on the inclination  
207 data, which provides a reliable magnetostratigraphy for most intervals. Identification and  
208 position of calcareous nannofossil events in 702B (Pea, 2011) and 1263 (Shipboard  
209 Scientific Party, 2004) (Fig. 2; Table S5) allow to clearly identify the magnetic chrons as  
210 C19r, C20n, C20r, C21n and C21r. Raw inclination, declination, and intensity data for  
211 each measurement step for ODP 1263 are given in Table S3. Magnetostratigraphic  
212 interpretation is given in Table S4. Processed paleomagnetic data from ODP 1263 basis  
213 for the magnetostratigraphic interpretation are provided in Table S9.

214

### 215 **3.3 Bulk stable isotope results**

216 The bulk carbon stable isotope data of Hole 702B (Fig. 2a) show a long-term increase  
217 from 0.8 to 2.0 ‰ in the interval Chron C21r to C18r. Site 1263 data (Fig. 2b) reveal a  
218 decrease from 2 to 1.6 ‰ from Chron C21r to C21n, an increase from 1.6 to 2 ‰ across  
219 the C20r/C21n boundary, a slight increase to 2.2 ‰ in the interval covering the mid  
220 Chron C20r to C20n, a decrease of 0.2 ‰ in Chron C20n, and an increasing trend in the  
221 early Chron C19r. The shift in carbon isotope data across the C20r/C21n boundary and  
222 the decrease in Chron C20n is very similar in both records pointing to global changes in  
223 the global carbon cycle. Both records show pronounced higher frequency variations  
224 related to short (100 kyr) and long (405 kyr) eccentricity cycles (see below).

225

226

#### 227 **4. Age Model development**

228 The age model for Sites 702 and 1263 was developed in a progressive series of steps.  
229 First, time series analysis was applied to the bulk  $\delta^{13}\text{C}$  data from both Sites 702 and 1263  
230 using evolutionary wavelet (Fig. 4) and MTM power spectra (Fig. S2 & S3). The Site 702  
231  $\delta^{13}\text{C}$  record is dominated by 6-8 m and  $\sim 2$  m cycles, whereas Site 1263 is dominated by  
232 3.5-4.5 m and  $\sim 1$  m cycles. Conversion to age applying the Geomagnetic Polarity Time  
233 Scale (GPTS) CK95 (Cande and Kent, 1995) reveals that these cycles correspond to the  
234 short ( $\sim 100$ -kyr) and long (405-kyr) eccentricity periods – similar to observations in early  
235 (Zachos et al., 2010) and late Eocene (Westerhold et al., 2014) deep-sea sediments.

236 Second, the dominant 405-kyr related cycles were extracted by band-pass filtering at the  
237 appropriate interval (Fig. 5; Site 702:  $0.16 \pm 0.048$  cyc/m; Site 1263: 155-180 rmc  
238  $0.29 \pm 0.087$  cyc/m, 180-230 rmc  $0.23 \pm 0.069$  cyc/m). After correlating the Site 702 and  
239 1263 records via magneto-stratigraphic tie points, a relative floating 405-kyr age model  
240 was established by counting cycles starting with 1 in the Site 1263 record at 158.60 rmc  
241 (Tab. S6). We determine a 2.6 to 2.7-Myr duration for magnetochron C20r and a 1.4-Myr  
242 duration for magnetochron C21n. Our new estimate for the duration of C20r is consistent  
243 with estimates from the standard CK95 (Cande and Kent, 1995) and GPTS2004 (Ogg and  
244 Smith, 2004) as well as a previous cyclostratigraphic estimate from the Contessa  
245 Highway section in Italy (Jovane et al., 2010), but is  $\sim 400$  kyr shorter than that estimated  
246 within the GPTS 2012 time scale (Ogg, 2012; Vandenberghe et al., 2012) (Fig. 5, Tables  
247 1-2).

248 Third, the floating 405-kyr age model was connected to the astronomical time scale  
249 (ATS) by correlation to ODP Site 1260 (Westerhold and Röhl, 2013; Westerhold et al.,  
250 2014) over magnetochron C20n (Fig. 6a). Site 1260 is tied to the cyclostratigraphic  
251 framework for the late middle Eocene-to-early Oligocene interval (Westerhold et al.,  
252 2014) and therefore establishes an independent bridge between the astronomically  
253 calibrated time scales of the Neogene to late Eocene and early Paleogene. The correlation  
254 and calibration of the cyclostratigraphic records from Sites 702 and 1263 place the

255 boundary of magnetochron C20n/C20r in 405-kyr Cycle 108 (43.5 Ma), the C20r/C21n  
256 boundary between 405-kyr Cycle 114 and 115 (~46.2 Ma), and the C21n/C21r boundary  
257 in 405-kyr cycle 118 (~47.6 Ma) (Fig. 5; Tables 1-2).

258 Fourth, because the orbital solutions La2010d and La2011 are valid back to ~50 Ma and  
259 the pattern of long and very long eccentricity cycle related components in both the Site  
260 702 and 1263 bulk  $\delta^{13}\text{C}$  records are very consistent with the La2010d and La2011 orbital  
261 solution for eccentricity, the carbon isotope records were minimally tuned to the La2011  
262 eccentricity by correlating lighter (more negative)  $\delta^{13}\text{C}$  peaks to eccentricity maxima  
263 (Fig. 5, (Ma et al., 2011)). This phase relationship has been observed in other deep-sea  
264  $\delta^{13}\text{C}$  bulk and benthic records (Pälike et al., 2006; Westerhold et al., 2014; Zachos et al.,  
265 2010) and thus is used here for the foundation of the tuning method (see supplementary  
266 material). The tie points to establish an astronomically tuned age model are shown in Fig.  
267 5 and listed in Table S10.

268 A potential issue in establishing a 405-kyr-based cyclostratigraphy is the missing or  
269 doubling of a 405-kyr cycle. Because the band-pass filter at Cycle 10 at Site 1263 shows  
270 a conspicuous cycle with a double hump (Fig. 5) and a stretched Cycle 9 at Site 702, we  
271 also provide an alternative 405-kyr age model with one additional 405-kyr cycle (18  
272 instead of 17 for the investigated interval of this study). Sedimentation rates calculated  
273 based on the 17 cycles-, the 18 cycles-, the magnetostratigraphic (using CK95) and the  
274 astronomical age model show a distinct drop using the 18 cycles model with respect to  
275 the other models (Fig. S5). Choosing the 18 cycles model would therefore lead to an  
276 unrealistically long duration for Chron C20r of more than 3.0 myr. In addition, the orbital  
277 solutions La2010d and La2011 are valid back to ~50 Ma and thus the match between the  
278 geological record and the astronomical solution as far as the expression of the 2.4 myr  
279 minima provides an important argument for rejecting the presence of a potential extra  
280 405-kyr cycle (Fig. 5). Based on these arguments we discarded the 18 405-kyr cycles  
281 model as an option.

282 By connecting the astronomically calibrated Site 1263  $\delta^{13}\text{C}$  record with the geochemical  
283 records of ODP Sites 1258 and 1262 we can extend the ATS into the early Paleogene up  
284 to the Cretaceous/Paleogene (K/Pg) boundary based on a continuous 405-kyr

286 cyclostratigraphic framework. This not only allows for comparison of the eccentricity  
287 related components in the geochemical records to the recent orbital solutions La2010 and  
288 La2011, but also provides accurate absolute ages for ash -17, the Paleocene-Eocene  
289 Thermal Maximum (PETM) and the K/Pg boundary independent from radio-isotopic  
290 dating and uncertainties in the 100-kyr and 2.4 myr eccentricity cycle components. Using  
291 bulk and benthic  $\delta^{13}\text{C}$  records as well as magnetostratigraphy, Site 1258 (Sexton et al.,  
292 2011) and Site 1263 (this study) can be tied together at 405-kyr Cycles 118 and 119 over  
293 the magnetochron C21n/C21r boundary (Fig. 6b). This establishes the connection of the  
294 early Paleogene cyclostratigraphies with the ATS of the Neogene and late Paleogene  
295 where all components of the orbital solutions are stable and uncertainties in radio-isotopic  
296 ages are very small. Closing the middle Eocene cyclostratigraphic gap establishes a  
297 complete and fully astronomically calibrated geological timescale for the Cenozoic and is  
298 the basis for extending the ATS into the Mesozoic.

299

300

## 301 **5. Discussion**

302 Integration of new and previously published results from ODP Sites 1258, 1260, 1262,  
303 and 1263 allows (i) placement of these records on a common 405-kyr cycle  
304 astronomically calibrated time scale across the middle Eocene, and (ii) evaluation of the  
305 evolution of Earth's eccentricity in the context of the latest generation of astronomical  
306 models for intervals older than 50 Ma.

307

### 308 **5.1 Consistent absolute ages for the Paleogene**

309 To assemble a complete Eocene GPTS, we combined the GPTS of the Pacific Equatorial  
310 Age Transect (PEAT, 31-41 Ma, C12n to C19n, (Westerhold et al., 2014)), of Site 1260  
311 (41-43 Ma, C19n to C20n, (Westerhold and Röhl, 2013)), Site 1263 (42-48 Ma, C20n-  
312 C21n, this study), and of Site 1258 (48-54 Ma, C21n-C24n, (Westerhold and Röhl,  
313 2009)) and updated to the age model established in this study (Tab. S11 & S12, Fig. 7).

314 The resulting Eocene GPTS covers magnetochron C12n to C24n and together with the  
315 recalibrated early (C29n to C27n, (Dinarès-Turell et al., 2014)) and late Paleocene (C26  
316 to C24r, Option 2 in (Westerhold et al., 2008)) as well as Oligocene (C6Cn to C12n,  
317 (Pälike et al., 2006)) it provides a full GPTS for the Paleogene period. The new tuned  
318 GPTS and the GPTS2012 (Ogg, 2012; Vandenberghe et al., 2012) are nearly consistent.  
319 Differences with respect to GPTS2012 are apparent in the duration of C20r, C22r and  
320 C23n.2n (Fig. 7A). The 2.634 myr duration for C20r interpreted in this study is consistent  
321 with estimates from the standard CK95 GPTS (Cande and Kent, 1995) and GPTS2004  
322 (Ogg and Smith, 2004) as well as a previous cyclostratigraphic estimate from the  
323 Contessa Highway section in Italy (Jovane et al., 2010). The difference for the duration of  
324 C20r to the estimate in GPTS2012 could be related to the selection of tie points for  
325 calibration of the GPTS. In GPTS2012 the astronomic age model with 6-order  
326 polynomial fit in the Eocene and the radio-isotopic age model give an absolute age for the  
327 top of C22n of 49.102 Ma and 48.570 Ma, respectively (Table 28.3 therein  
328 (Vandenberghe et al., 2012)). This difference of 536 kyr mirrors the uncertainty in this  
329 interval of the time scale GPTS2012. However, the radio-isotopic ages are primarily used  
330 for the final age model in GPTS2012 from C16r to top of C24n.1n (37-53 Ma,  
331 (Vandenberghe et al., 2012)). GPTS2012 uses the Mission Valley ash near base of C20n  
332 with  $^{40}\text{Ar}/^{39}\text{Ar}$  age of 43.35 Ma which is consistent with our tuned age of 43.517 Ma for  
333 the base of C20n. Because of the relatively large error in the next calibration point (an ash  
334 horizon in DSDP Hole 516F at C21n.75 with an age of  $46.24 \pm 0.5$  Ma (Vandenberghe et  
335 al., 2012)) the duration of C20r in GPTS2012 (2.292 myr) has to be considered with  
336 caution. The differences in duration of C22r and C23n.2n (~400-kyr longer C22r; ~400-  
337 kyr shorter C23n.2n) could be related to the difficult interpretation of the Site 1258  
338 magnetostratigraphy (Westerhold and Röhl, 2009) and require recovery of additional  
339 high-quality records from deep-sea successions in the future for confirmation. This  
340 uncertainty in the duration of C22r and C23n.2n at Site 1258 does not affect the number  
341 of 405-kyr cycles identified in this record, but is the result of uncertainties in determining  
342 the exact position of the magnetic reversal. [This is complicated by the rather large error](#)  
343 [in the width of the magnetic anomaly profiles for C21r \(12.8%\), C22r \(11.9%\) and C23](#)  
344 [\(17.3%\) \(Cande and Kent, 1992; Tab. 4 therein\) which results in very uncertain durations](#)

345 [for chrons \(see Table S13\). Combining both the error in absolute age for the calibration](#)  
346 [tie points \(ash layers, boundaries\) and the error in the exact placement of boundaries](#)  
347 [between marine magnetic anomalies in the CK95 model \(Table S13\) it is clear that the](#)  
348 [determination of the exact durations of magnetochrons is much more difficult than](#)  
349 [assumed in many publications. Once the durations for C21r, C22r and C23 based on the](#)  
350 [ODP Site 1258 cyclostratigraphy are evaluated by an additional high-resolution bio-](#)  
351 [magneto- and cyclostratigraphy on another site, the resulting new precise cycle-durations](#)  
352 [for chrons could help to provide an improved estimate for the deep-seas magnetic](#)  
353 [anomaly widths as in CK95.](#)

354 Previous correlation of geological data to the La2011 orbital solution led to a discrepancy  
355 between astronomical and radio-isotopic  $^{40}\text{Ar}/^{39}\text{Ar}$  ages of ash -17 (Storey et al., 2007)  
356 derived from Deep Sea Drilling Project (DSDP) Site 550 (Knox, 1984) and the age of the  
357 Paleocene-Eocene Thermal Maximum (PETM) (Vandenbergh et al., 2012; Westerhold  
358 et al., 2012; Westerhold et al., 2009). Linking the published cyclostratigraphies for the  
359 Paleocene (Westerhold et al., 2008) and early to middle Eocene (Westerhold and Röhl,  
360 2009; Westerhold et al., 2012; Westerhold et al., 2007) to our ATS across the C21n/C21r  
361 boundary in 405-kyr Cycle 118 at ~47.6 Ma (Fig. 6b) clearly shows that only Option 2  
362 (Westerhold et al., 2012; Westerhold et al., 2007) of the early-to-middle Eocene floating  
363 cyclostratigraphies is consistent with our new astronomically tuned age for C21n/C21r  
364 boundary. Our records spanning the middle Eocene cyclostratigraphic gap provide an  
365 absolute age estimate of 55.280 Ma for ash -17 and the onset of the PETM in 405-kyr  
366 Cycle 139 at 55.930 Ma, as in Option 2 of the astronomically calibrated Paleocene time  
367 scale (Westerhold et al., 2008). This age for the onset of the PETM is consistent with a  
368 high-precision radio-isotopic U/Pb age of 55.728–55.964 Ma from bentonite layers  
369 within the PETM interval at Spitzbergen (Charles et al., 2011). The absolute age for the  
370 onset of the PETM confirmed here at 55.930 Ma is also synchronous with the initiation of  
371 North Atlantic flood basalt volcanism (Skaergaard intrusion at  $55.960 \pm 0.064$  Ma,  
372 (Wotzlaw et al., 2012)).

373 After revision of the Paleocene cyclostratigraphy from deep-sea data (Dinarès-Turell et  
374 al., 2014) showing that the Paleocene spans 25 (Hilgen et al., 2010) and not 24  
375 (Westerhold et al., 2008) 405-kyr cycles and with the complete stratigraphic framework

376 now at hand we provide absolute astronomical ages for key events in the Eocene and  
377 Paleocene for reference (Table 3). Updates for ages of magnetochron boundaries await  
378 solving the uncertainties for the durations of Chrons C22n to C23r. Our complete  
379 framework confirms the astronomically calibrated age of the K/Pg boundary of  $66.022 \pm$   
380  $0.040$  Ma (Dinarès-Turell et al., 2014). This is consistent with a recent high-precision  
381 radio-isotopic U/Pb age for the K/Pg boundary of  $66.038$  Ma (Renne et al., 2013). The  
382 major uncertainty in age estimates stems from uncertainties in the exact absolute age  
383 assignment of the 405-kyr eccentricity maxima at 56 and 66 Ma. According to (Laskar et  
384 al., 2011a; Laskar et al., 2011b) the error at 56 Ma is in the order of 50 kyr and at 66 Ma  
385 in the order of 60 kyr.

386 The age astronomically calibrated age for ash -17 of  $55.280$  Ma is inconsistent with  
387  $^{40}\text{Ar}/^{39}\text{Ar}$  ages using the most recent age calibrations for the FCT dating standard monitor  
388 of  $28.201$  (Kuiper et al., 2008),  $28.305$  (Renne et al., 2010),  $27.93$  (Channell et al., 2010),  
389  $27.89$  (Westerhold et al., 2012), and  $28.172$  (Rivera et al., 2011) Ma (Fig. S7). Assuming  
390 that the  $55.280$  Ma age for ash -17 is correct we calculate an absolute age of  $\sim 28.10$  Ma  
391 for the FCT monitor which is within the error of the  $28.172$  (Rivera et al., 2011) Ma  
392 estimate. The age of  $28.10$  Ma for the FCT leads to an age for the highly reproducible  
393 inter-laboratory  $^{40}\text{Ar}/^{39}\text{Ar}$  measurements made on the Beloc tektite at the K/Pg boundary  
394 that is more than 400 kyr younger than the highly accurate U/Pb age (Renne et al., 2013)  
395 contradicting the rock clock synchronization (Kuiper et al., 2008). Independent  
396 confirmation of the  $\sim 28.2$  Ma astronomically calibrated age for the FCT (Kuiper et al.,  
397 2008; Rivera et al., 2011; Wotzlav et al., 2014) and the absolute age of the K/Pg  
398 boundary of  $66.022$  Ma (Dinarès-Turell et al., 2014; Kuiper et al., 2008; Renne et al.,  
399 2013) place doubt on the astronomically calibrated age for ash -17. Both the geochemical  
400 identification of ash -17 in ODP Site 550 (Knox, 1984) and the relative distance to the  
401 onset of the PETM (Westerhold et al., 2009) need revision before any evaluation can be  
402 done.

403

## 404 [5.2 Terrestrial vs deep-sea GPTS](#)

Autor

Gelöscht: 6

406 [High-resolution radio-isotopic dating of Eocene terrestrial strata, from the Green River](#)  
407 [Formation in particular, has been utilized during the last 20 years towards improving the](#)  
408 [Eocene GPTS](#) (Clyde et al., 2004; Clyde et al., 2001; Clyde et al., 1997; Machlus et al.,  
409 2004; Machlus et al., 2008; Machlus et al., 2015; Shipboard Scientific Party, 1988; Smith  
410 et al., 2008a; Smith et al., 2008b; Smith et al., 2010; Smith et al., 2003; Smith et al.,  
411 2006; Smith et al., 2004; Tsukui and Clyde, 2012; Westerhold and Röhl, 2009). [Although](#)  
412 [one must state that the correlation of terrestrial sections and accurate age dating of ash](#)  
413 [layers is highly complex we evaluate our new GPTS in comparison with to the terrestrial](#)  
414 [calibrations \(Fig. 7a\). Focusing on the latest Green River Formation GPTS calibrations](#)  
415 [\(all adjusted and reported by Smith et al. \(2010\) and Tsukui & Clyde \(2012\) to FCT](#)  
416 [28.201 Ma of Kuiper et al. \(2008\)\), it becomes very clear that substantial differences in](#)  
417 [calibration and interpretation exist that are based on very similar data sets.](#)

418 [Because most of the radio-isotopic dates for ash layers in the Green River Formation are](#)  
419 [established on  \$^{40}\text{Ar}/^{39}\text{Ar}\$  ages, they are directly dependent on the absolute age of the FCT](#)  
420 [standard \(see discussion in Westerhold & Röhl \(2009\) and Westerhold et al. \(2012\)\).](#)  
421 [High quality U/Pb ages are also available for some ash layers \(Smith et al. 2010 \[Analcite](#)  
422 [and Firehole tuff\] and Machlus et al. 2015 \[Sixth, Layered, Main, Grey, Second, Firehole](#)  
423 [and 1448 Tuff\]\). The Firehole tuff has a consistent U/Pb age of  \$51.66 \pm 0.19\$  Ma in Smith](#)  
424 [et al. \(2010\) and  \$51.528 \pm 0.061\$  Ma in Machlus et al. \(2015\). The  \$^{40}\text{Ar}/^{39}\text{Ar}\$  age of the](#)  
425 [Firehole Tuff is  \$51.40 \pm 0.25\$  Ma \(FCT 28.201 Ma\) \(Smith et al. 2010\). The Firehole tuff,](#)  
426 [however, was not included by Smith et al. \(2010\) for recalibrating the GPTS. According](#)  
427 [to Tsukui & Clyde \(2015\) the Firehole tuff is in a paleomagnetic reversal, likely C23r](#)  
428 [\(see Table DR4 in Tsukui & Clyde 2012\). Unfortunately, the Analcite Tuff \(U/Pb  \$49.23 \pm\$](#)   
429 [0.12 Ma, Smith et al. 2010\) has not clear paleomagnetic polarity \(Tsukui & Clyde 2015\).](#)  
430 [Comparing the radioisotopic ages used by Smith et al. \(2010\) and their paleomagnetic](#)  
431 [pattern with the astronomically calibrated GPTS \(Fig. 7a\) shows consistent results for the](#)  
432 [Mission Valley ash \(in C20n\), the Montanari ash \(in C21n\), the Blue Point Marker ash \(in](#)  
433 [C21r\), the Continental tuff \(in C22n\), the Firehole tuff \(in C23r\) and the Willwood ash](#)  
434 [\(in C24n\). Inconsistencies are apparent for the Sixth tuff and Layered tuff which have a](#)  
435 [normal polarity but correlate to C22r in the astronomical GPTS.](#)

436 [Tsukui & Clyde \(2012\)](#) utilized more ash layers for their calibration that has substantial  
437 differences to the GPTS by [Smith et al. \(2010\)](#) from C21n to C24n (Fig. 7b). Some ash  
438 layers, for example, in C21r and C23n of the GPTS of [Tsukui & Clyde \(2012\)](#), have an  
439 opposite polarity although they are of similar age. The GPTS of [Tsukui & Clyde \(2012\)](#)  
440 is more consistent with the astronomical GPTS for Chron C22 and C23, but the Sixth ash,  
441 the Layered tuff and the Main tuff occur in an interval of normal polarity correlate to  
442 C22r in the astronomical GPTS. In contrast, the Firehole tuff, located in an interval of  
443 reversed polarity, is positioned in C23n according to the GPTS of [Tsukui & Clyde](#)  
444 [\(2012\)](#). We would argue that the duration of C23n as estimated by [Tsukui & Clyde](#)  
445 [\(2012\)](#) is probably too long. A detailed comparison of the GPTS for Chrons C22 and C23  
446 between terrestrial and deep-sea records is difficult at the moment because the deep-sea  
447 and the terrestrial GPTS still need to be examined in detail in the early Eocene, as  
448 described above. The error in the mean width of the anomaly profile defined by [Cande](#)  
449 [and Kent \(1992, Table 4 therein\)](#) for C21r, C22r and C23 is between 12 and 17% (Table  
450 S13), which can also help to explain larger differences in durations between the terrestrial  
451 and deep-sea records. A new deep-sea magneto-cyclostratigraphic record is needed to test  
452 the ODP Site 1258 results in order to validate the duration of magnetochrons C22 and  
453 C23. Nevertheless, it seems that these records align for Chron C24n suggesting that both  
454 astrochronology and radio-isotopic dating of terrestrial successions are in agreement for  
455 at least this time interval. A more detailed comparison between marine and terrestrial  
456 records is well beyond the scope of this paper, a more in-depth synthesis and discussion  
457 of terrestrial and deep-sea GPTS for the Eocene has to be addressed by a future synthesis  
458 similar to the Paleogene chapter in the GTS2012 ([Vandenbergh et al., 2012](#)).

459

### 460 **5.3 Stability of orbital solutions**

461 The new  $\delta^{13}\text{C}$  records from Sites 702 and 1263 reveal low amplitude variations in 405-  
462 kyr cycles 4, 10 and 16 (Fig. 5), which likely coincide with minima in eccentricity  
463 amplitude modulation occurring approximately every 2.4 Myr ([Laskar et al., 2004](#)). The  
464 2.4-Myr cycle in the amplitude modulation of geological data and orbital eccentricity are  
465 consistent up to 48–49 Ma (Fig. S6). In older time intervals, the geological data and

Autor

Gelöscht: 5

467 orbital solution are out of sync suggesting that the short and very long eccentricity  
468 component in orbital solutions are correct only back to 48 Ma, but not to 52-54 Ma as  
469 previously thought (Westerhold et al., 2012). This implies that only the stable 405-kyr  
470 eccentricity pattern in the La2010 and La2011 solutions can be used for direct  
471 astronomical calibration for periods older than 48-50 Ma. Because the orbital solutions  
472 La2010d and La2011 (Laskar et al., 2011a; Laskar et al., 2011b) show an excellent fit to  
473 the internally-anchored  $\delta^{13}\text{C}$  records the long-term behavior of the INPOP10a  
474 (Intégration Numérique Planétaire de l'Observatoire de Paris, (Fienga et al., 2011))  
475 ephemeris used for La2010d and La2011 can be considered more stable than that of the  
476 INPOP08 (Fienga et al., 2009) ephemeris.

477 The divergence between geological data and astronomical solutions beyond 48-50 Ma has  
478 strong implications for the La2010 (Laskar et al., 2011a) and La2011 (Laskar et al.,  
479 2011b) orbital models. Both models propose a transition from libration to circulation  
480 appearing around 50 Ma in the resonant argument related to  $\theta = (s_4 - s_3) - 2(g_4 - g_3)$ ,  
481 the combination of angles in the precession motion of the orbits of Earth and Mars  
482 (Laskar et al., 2004; Pälike et al., 2004). [Identifying this transition is of high importance](#)  
483 [because it would provide direct evidence of the chaotic, not quasiperiodic, nature of the](#)  
484 [solar system](#) (Laskar, 1989) [and set the conditions for the gravitational model of the Solar](#)  
485 [System](#) (Laskar et al., 2004). [In modern planetary ephemeris the initial conditions are](#)  
486 [obtained by least-squares fittings to large sets of observational data](#) (Fienga et al., 2008)  
487 [and thus depend on the accuracy of these data. The point in time when the transition from](#)  
488 [libration to circulation occurs is sensitive to the initial conditions of the planetary](#)  
489 [ephemeris solutions. In geological records](#) the chaotic diffusion will be expressed as a  
490 prominent change from a  $\sim 2.4$ -Myr to a very regular 2.0-Myr periodicity in the very long  
491 eccentricity cycle (Laskar et al., 2004; Pälike et al., 2004). Due to irregular spacing from  
492 4 to 6 long eccentricity cycles between very long eccentricity minima in the geological  
493 data from 50 to 60 Ma the chaotic diffusion of the orbital trajectories as proposed in  
494 La2010d and La2011 cannot be verified (Fig. S6). This major discrepancy points to  
495 inaccuracy in the planetary ephemeris solutions, which are currently limited due to the  
496 chaotic behavior of the large asteroids (Laskar et al., 2011b). The transition from libration  
497 to circulation needs to be identified in older geological intervals to help to refine orbital

499 models. A precise calculation of Earth's eccentricity beyond 60 Ma is not possible  
500 (Laskar et al., 2011b) but geological data, preferably stable carbon isotope data, from 50  
501 to 100 Ma could help to detect this critical transition and provide important information  
502 for future orbital models.

Autor

Gelöscht: e.g.

503

504

## 505 **6 Conclusions**

506 The closing of the middle Eocene gap and the connection of the 405-kyr  
507 cyclostratigraphies of the Eocene and Paleocene complete a fully astronomically  
508 calibrated geological timescale for the Cenozoic. Derived absolute ages for the PETM  
509 and K/Pg boundary are now consistent with the intercalibration of radio-isotopic and  
510 astronomical dating methods. Previous discrepancies lie in the uncertainties of orbital  
511 solutions beyond 50 Ma and problems in the determination of the absolute age of ash -17  
512 in the early Eocene with respect to cyclostratigraphy (Hilgen et al., 2010; Storey et al.,  
513 2007; Westerhold et al., 2009). The new accurate stratigraphy is a key to explore why and  
514 how Earth climate shifted from a greenhouse to an icehouse climate state throughout the  
515 Paleogene [in unprecedented detail. Comparison of terrestrial and deep-sea calibrations of  
516 the GPTS suggests that ages and durations of Chrons C22 and C23 need to be studied in  
517 more detail to solve current discrepancies in the future. The presently observed  
518 differences in Chrons C22 and C23 stem from uncertainties in the exact width of the  
519 stacked deep-sea anomaly profile of Cande and Kent \(1992\), the lack of good quality  
520 magnetostratigraphy from deep-sea records, and uncertainties in the position as well as  
521 age of some ash layers in the terrestrial Green River Formation.](#) Importantly the  
522 comparison between bulk carbonate carbon isotope data and orbital models for Earth's  
523 eccentricity reveal inaccuracy in the planetary ephemeris solutions and limit direct  
524 astronomical calibration using the short eccentricity cycle to 48 Ma.

Autor

Gelöscht: in unprecedented detail

Autor

Gelöscht: in

525

526

## 527 **Acknowledgments**

531 We thank Monika Segl and her team for stable isotope analyses at MARUM, Alexander  
532 Houben and Dyke Andreasen for stable isotope analyses at UCSC, Roy Wilkens  
533 (University of Hawaii) for introducing us into the world of core image analysis, Alex  
534 Wülbers and Walter Hale at the IODP Bremen Core Repository for core handling, and  
535 Vera Lukies (MARUM) for assistance with XRF core scanning. This research used  
536 samples and data provided by the International Ocean Discovery Program (IODP). IODP  
537 is sponsored by the US National Science Foundation (NSF) and participating countries.  
538 Financial support for this research was provided by the Deutsche  
539 Forschungsgemeinschaft (DFG). The data reported in this paper are tabulated in the  
540 Supporting Online Material and archived at the Pangaea ([www.pangaea.de](http://www.pangaea.de)) database.  
541 T.W. and U.R. designed the study, generated stable bulk isotope data for ODP Site 1263,  
542 and applied time series analysis. T. F. conducted the paleomagnetic analysis. S.B.  
543 generated the bulk isotope data for ODP Site 702, and J.Z. generated bulk isotope data for  
544 1263. T.W., U.R., T. F., S.B. and J.Z. interpreted the data and wrote the paper.

545

## 546 **References**

- 547 Aubry, M. P.: From Chronology to Stratigraphy: Interpreting the Lower and Middle Eocene Stratigraphic  
548 Record in the Atlantic Ocean, in: *Geochronology, Time Scales and Global Stratigraphic Correlation*,  
549 edited by: Berggren, W. A., Kent, D. V., Aubry, M. P., and Hardenbol, J., SEPM, Spec. Publ., 213-274,  
550 10.2110/pec.95.04.0213, 1995.
- 551 Cande, S. C., and Kent, D. V.: A New Geomagnetic Polarity Time Scale for the late Cretaceous and  
552 Cenozoic, *Journal of Geophysical Research*, 97, 13,917-913,951, 1992.
- 553 Cande, S. C., and Kent, D. V.: Revised calibration of the geomagnetic polarity timescale for the Late  
554 Cretaceous and Cenozoic, *Journal of Geophysical Research*, 100, 6093-6095, 1995.
- 555 Channell, J. E. T., Hodell, D. A., Singer, B. S., and Xuan, C.: Reconciling astrochronological and  $^{40}\text{Ar}/^{39}\text{Ar}$   
556 ages for the Matuyama-Brunhes boundary and late Matuyama Chron, *Geochem. Geophys. Geosyst.*, 11,  
557 21, 10.1029/2010GC003203 2010.
- 558 Charles, A. J., Condon, D. J., Harding, I. C., Pälike, H., Marshall, J. E. A., Cui, Y., Kump, L., and  
559 Croudace, I. W.: Constraints on the numerical age of the Paleocene-Eocene boundary, *Geochem.*  
560 *Geophys. Geosyst.*, 12, Q0AA17, 10.1029/2010gc003426, 2011.
- 561 Clement, B. M., and Hailwood, E. A.: Magnetostratigraphy of sediments from Sites 701 and 702, in: *Proc.*  
562 *ODP, Sci. Results*, 114: College Station, TX (Ocean Drilling Program), edited by: Ciesielski, P. F.,  
563 Kristoffersen, Y., and et al., 359-366, 10.2973/odp.proc.sr.114.156.1991, 1991. Place: College Station,  
564 TX, Publisher: Ocean Drilling Program, Texas A&M University
- 565 Clyde, W. C., Zonneveld, J.-P., Stamatakos, J., Gunnell, Y., and Bartels, W. S.: Magnetostratigraphy across  
566 the Wasatchian/Bridgerian NALMA Boundary (Early to Middle Eocene) in the Western Green River  
567 Basin, Wyoming, *Journal of Geology*, 150, 657-669, 1997.
- 568 Clyde, W. C., Sheldon, N. D., Koch, P. L., Gunnell, G. F., and Bartels, W. S.: Linking the  
569 Wasatchian/Bridgerian boundary to the Cenozoic Global Climate Optimum: new magnetostratigraphic  
570 and isotopic results from South Pass, Wyoming, *Palaeogeography, Palaeoclimatology, Palaeoecology*,  
571 167, 175-199, 2001.

572 Clyde, W. C., Bartels, W. S., Gunnell, G. F., and Zonneveld, J.-P.: 40Ar/39Ar geochronology of the  
573 Eocene Green River Formation, Wyoming: Discussion, Geological Society of America Bulletin, 116,  
574 251-252, 2004.

575 Dinarès-Turell, J., Westerhold, T., Pujalte, V., Röhl, U., and Kroon, D.: Astronomical calibration of the  
576 Danian stage (Early Paleocene) revisited: Settling chronologies of sedimentary records across the  
577 Atlantic and Pacific Oceans, Earth and Planetary Science Letters, 405, 119-131,  
578 10.1016/j.epsl.2014.08.027, 2014.

579 Fienga, A., Manche, H., Laskar, J., and Gastineau, M.: INPOP06: a new numerical planetary ephemeris,  
580 Astronomy & Astrophysics, 477, 315-327, 10.1051/0004-6361/20066607, 2008.

581 Fienga, A., Laskar, J., Morley, T., Manche, H., Kuchynka, P., Le Poncin-Lafitte, C., Budnik, F., Gastineau,  
582 M., and Somenzi, L.: INPOP08, a 4-D planetary ephemeris: from asteroid and time-scale computations  
583 to ESA Mars Express and Venus Express contributions, Astronomy & Astrophysics, 507, 1675-1686,  
584 10.1051/0004-6361/200911755, 2009.

585 Fienga, A., Laskar, J., Kuchynka, P., Manche, H., Desvignes, G., Gastineau, M., Cognard, I., and Theureau,  
586 G.: The INPOP10a planetary ephemeris and its applications in fundamental physics Celestial Mechanics  
587 and Dynamical Astronomy, 111, 363-385, 10.1007/s10569-011-9377-8, 2011.

588 Ghil, M., Allen, M. R., Dettinger, M. D., Ide, K., Kondrashov, D., Mann, M. E., Robertson, A. W.,  
589 Saunders, A., Tian, Y., Varadi, F., and Yiou, P.: Advanced Spectral Methods for Climatic Time Series,  
590 Reviews of Geophysics, 40, 1003, 10.1029/2000RG000092, 2002.

591 Hilgen, F. J.: Astronomical dating in the 19th century, Earth-Science Reviews, 98, 65-80,  
592 10.1016/j.earscirev.2009.10.004, 2010.

593 Hilgen, F. J., Kuiper, K. F., and Lourens, L. J.: Evaluation of the astronomical time scale for the Paleocene  
594 and earliest Eocene, Earth and Planetary Science Letters, 300, 139-151, 10.1016/j.epsl.2010.09.044,  
595 2010.

596 Hilgen, F. J., Abels, H. A., Kuiper, K. F., Lourens, L. J., and Wolthers, M.: Towards a stable astronomical  
597 time scale for the Paleocene: Aligning Shatsky Rise with the Zumaia – Walvis Ridge ODP Site 1262  
598 composite, Newsletters on Stratigraphy, 48, 91-110, 10.1127/nos/2014/0054, 2015.

599 Hinnov, L. A., and Hilgen, F. J.: Chapter 4 - Cyclostratigraphy and Astrochronology, in: The Geologic  
600 Time Scale, edited by: Gradstein, F. M., Ogg, J. G., Schmitz, M. D., and Ogg, G. M., Elsevier, Boston,  
601 63-83, <http://dx.doi.org/10.1016/B978-0-444-59425-9.00004-4>, 2012.

602 Hinnov, L. A.: Cyclostratigraphy and its revolutionizing applications in the earth and planetary sciences,  
603 Geological Society of America Bulletin, 125, 1703-1734, 10.1130/b30934.1, 2013.

604 Jovane, L., Sprovieri, M., Coccioni, R., Florindo, F., Marsili, A., and Laskar, J.: Astronomical calibration  
605 of the middle Eocene Contessa Highway section (Gubbio, Italy), Earth and Planetary Science Letters,  
606 298, 77-88, 10.1016/j.epsl.2010.07.027, 2010.

607 Kirschvink, J. L.: The least-squares line and plane and the analysis of paleomagnetic data, Geophys. J. Roy.  
608 Astron. Soc., 62, 699-718, 10.1111/j.1365-246X.1980.tb02601.x, 1980.

609 Knox, R. W. O. B.: Nannoplankton zonation and the Palaeocene/Eocene boundary beds of NW Europe: an  
610 indirect correlation by means of volcanic ash layers, Journal of the Geological Society, 141, 993-999,  
611 10.1144/gsjgs.141.6.0993, 1984.

612 Kuiper, K. F., Deino, A., Hilgen, F. J., Krijgsman, W., Renne, P. R., and Wijbrans, J. R.: Synchronizing  
613 Rock Clocks of Earth History, Science, 320, 500-504, 10.1126/science.1154339, 2008.

614 Laskar, J.: A numerical experiment on the chaotic behaviour of the Solar System, Nature, 338, 237-238,  
615 1989.

616 Laskar, J., Robutel, P., Joutel, F., Gastineau, M., Correia, A., and Levrard, B.: A long-term numerical  
617 solution for the insolation quantities of the Earth, Astronomy and Astrophysics, 428, 261-285,  
618 10.1051/0004-6361/20041335, 2004.

619 Laskar, J., Fienga, A., Gastineau, M., and Manche, H.: La2010: a new orbital solution for the long-term  
620 motion of the Earth, Astronomy and Astrophysics, 532, A89, 10.1051/0004-6361/201116836, 2011a.

621 Laskar, J., Gastineau, M., Delisle, J. B., Farrés, A., and Fienga, A.: Strong chaos induced by close  
622 encounters with Ceres and Vesta, Astronomy and Astrophysics, 532, L4, 10.1051/0004-  
623 6361/201117504, 2011b.

624 Lourens, L. J., Hilgen, F. J., Laskar, J., Shackleton, N. J., and Wilson, D.: The Neogene Period, in: A  
625 Geological Timescale 2004, edited by: Gradstein, F., Ogg, J., and Smith, A., 409-440,  
626 10.1017/CBO9780511536045.022, 2004, Cambridge University Press, UK

627 Lurcock, P. C., and Wilson, G. S.: PuffinPlot: A versatile, user-friendly program for paleomagnetic  
628 analysis, *Geochemistry, Geophysics, Geosystems*, 13, Q06Z45, 10.1029/2012GC004098, 2012.

629 Ma, W., Tian, J., Li, Q., and Wang, P.: Simulation of long eccentricity (400-kyr) cycle in ocean carbon  
630 reservoir during Miocene Climate Optimum: Weathering and nutrient response to orbital change,  
631 *Geophysical Research Letters*, 38, L10701, 10.1029/2011GL047680, 2011.

632 Machlus, M., Hemming, S. R., Olsen, P. E., and Christie-Blick, N.: Eocene calibration of geomagnetic  
633 polarity time scale reevaluated: Evidence from the Green River Formation of Wyoming, *Geology*, 32,  
634 137-140, 10.1130/G20091.1, 2004.

635 Machlus, M. L., Olsen, P. E., Christie-Blick, N., and Hemming, S. R.: Spectral analysis of the lower  
636 Eocene Wilkins Peak Member, Green River Formation, Wyoming: Support for Milankovitch cyclicity,  
637 *Earth and Planetary Science Letters*, 268, 64-75, 2008.

638 Machlus, M. L., Ramezani, J., Bowring, S. A., Hemming, S. R., Tsukui, K., and Clyde, W. C.: A strategy  
639 for cross-calibrating U–Pb chronology and astrochronology of sedimentary sequences: An example  
640 from the Green River Formation, Wyoming, USA, *Earth and Planetary Science Letters*, 413, 70-78,  
641 <http://dx.doi.org/10.1016/j.epsl.2014.12.009>, 2015.

642 Mann, M. E., and Lees, J. M.: Robust estimation of background noise and signal detection in climatic time  
643 series, *Climatic Change*, 33, 409-445, 10.1007/BF00142586, 1996.

644 Ogg, J. G., and Bardot, L.: Aptian through Eocene magnetostratigraphic correlation of the Blake Nose  
645 Transect (Leg 171B), Florida Continental Margin, in: *Proc. ODP, Sci. Results, 171B: College Station,  
646 TX (Ocean Drilling Program)*, edited by: Kroon, D., Norris, R. D., and Klaus, A., 1-58,  
647 10.2973/odp.proc.sr.171b.104.2001, 2001. Place: College Station, TX, Publisher: Ocean Drilling  
648 Program, Texas A&M University

649 Ogg, J. G., and Smith, A. G.: The geomagnetic polarity time scale, in: *A Geological Timescale 2004*, edited  
650 by: Gradstein, F., Ogg, J., and Smith, A., Cambridge University Press, UK, 63-86, 2004

651 Ogg, J. G.: Chapter 5 - Geomagnetic Polarity Time Scale, in: *The Geologic Time Scale*, edited by:  
652 Gradstein, F. M., Ogg, J. G., Schmitz, M. D., and Ogg, G. M., Elsevier, Boston, 85-113,  
653 <http://dx.doi.org/10.1016/B978-0-444-59425-9.00005-6>, 2012.

654 Pälike, H., Laskar, J., and Shackleton, N. J.: Geologic constraints on the chaotic diffusion of the solar  
655 system, *Geology*, 32, 929-932, 10.1130/G20750.1, 2004.

656 Pälike, H., Norris, R. D., Herrle, J. O., Wilson, P. A., Coxall, H. K., Lear, C. H., Shackleton, N. J., Tripathi,  
657 A. K., and Wade, B. S.: The Heartbeat of the Oligocene Climate System, *Science*, 314, 1894-1898,  
658 10.1126/science.1133822, 2006.

659 Pälike, H., and Hilgen, F.: Rock clock synchronization, *Nature Geosci*, 1, 282-282, 10.1038/ngeo197, 2008.

660 Pea, L.: Eocene-Oligocene paleoceanography of the subantarctic South Atlantic: Calcareous Nannofossil  
661 reconstructions of temperature, nutrient, and dissolution history, PhD., University of Parma, Parma,  
662 Italy, 205 pp., 2011.

663 Phillips, D., and Matchan, E. L.: Ultra-high precision  $^{40}\text{Ar}/^{39}\text{Ar}$  ages for Fish Canyon Tuff and Alder Creek  
664 Rhyolite sanidine: New dating standards required?, *Geochimica et Cosmochimica Acta*, 121, 229-239,  
665 <http://dx.doi.org/10.1016/j.gca.2013.07.003>, 2013.

666 Renne, P. R., Swisher, C. C., Deino, A. L., Karner, D. B., Owens, T. L., and DePaolo, D. J.: Intercalibration  
667 of standards, absolute ages and uncertainties in  $^{40}\text{Ar}/^{39}\text{Ar}$  dating, *Chemical Geology*, 145, 117-152,  
668 1998.

669 Renne, P. R., Mundil, R., Balco, G., Min, K., and Ludwig, K. R.: Joint determination of  $^{40}\text{K}$  decay  
670 constants and  $^{40}\text{Ar}/^{40}\text{K}$  for the Fish Canyon sanidine standard, and improved accuracy for  $^{40}\text{Ar}/^{39}\text{Ar}$   
671 geochronology, *Geochimica et Cosmochimica Acta*, 74, 5349-5367, 10.1016/j.gca.2010.06.017, 2010.

672 Renne, P. R., Deino, A. L., Hilgen, F. J., Kuiper, K. F., Mark, D. F., Mitchell, W. S., Morgan, L. E.,  
673 Mundil, R., and Smit, J.: Time Scales of Critical Events Around the Cretaceous-Paleogene Boundary,  
674 *Science*, 339, 684-687, 10.1126/science.1230492, 2013.

675 Rivera, T. A., Storey, M., Zeeden, C., Hilgen, F. J., and Kuiper, K.: A refined astronomically calibrated  
676  $^{40}\text{Ar}/^{39}\text{Ar}$  age for Fish Canyon sanidine, *Earth and Planetary Science Letters*, 311, 420-426,  
677 10.1016/j.epsl.2011.09.017, 2011.

678 Sexton, P. F., Norris, R. D., Wilson, P. A., Pälike, H., Westerhold, T., Röhl, U., Bolton, C. T., and Gibbs,  
679 S.: Eocene global warming events driven by ventilation of oceanic dissolved organic carbon, *Nature*,  
680 471, 349-352, 10.1038/nature09826, 2011.

681 Shipboard Scientific Party: Site 702, in: Proc. ODP, Init. Repts., 114: College Station, TX (Ocean Drilling  
682 Program), edited by: Ciesielski, P. F., Kristoffersen, Y., and et al., 10.2973/odp.proc.ir.114.109.1988,  
683 1988, Place: College Station, TX, Publisher: Ocean Drilling Program, Texas A&M University  
684 Shipboard Scientific Party: Site 1263, in: Proc. ODP, Init. Repts., 208: College Station, TX (Ocean Drilling  
685 Program), edited by: Zachos, J. C., Kroon, D., Blum, P., and et al., 1-87,  
686 10.2973/odp.proc.ir.208.104.2004, 2004, Place: College Station, TX, Publisher: Ocean Drilling  
687 Program, Texas A&M University  
688 Smith, E. M., Carroll, A. R., and Mueller, E. R.: Elevated weathering rates in the Rocky Mountains during  
689 the Early Eocene Climatic Optimum, *Nature Geosci*, 1, 370-374, 10.1038/ngeo205, 2008a.  
690 Smith, M. E., Singer, B., and Carroll, A.: 40Ar/39Ar geochronology of the Eocene Green River Formation,  
691 Wyoming, *GSA Bulletin*, 115, 549-565, 10.1130/0016-7606(2003)115, 2003.  
692 Smith, M. E., Singer, B. S., and Carroll, A. R.: Reply, *Geological Society of America Bulletin*, 116, 253-  
693 256, 2004.  
694 Smith, M. E., Singer, B., Carroll, A., and Fournelle, J. H.: High-resolution calibration of Eocene strata:  
695 40Ar/39Ar geochronology of biotite in the Green River Formation, *Geology*, 32, 393-396,  
696 10.1130/G22265.1, 2006.  
697 Smith, M. E., Carroll, A. R., and Singer, B. S.: Synoptic reconstruction of a major ancient lake system:  
698 Eocene Green River Formation, western United States, *Geological Society of America Bulletin*, 120,  
699 54-84, 2008b.  
700 Smith, M. E., Chamberlain, K. R., Singer, B. S., and Carroll, A. R.: Eocene clocks agree: Coeval  
701 40Ar/39Ar, U-Pb, and astronomical ages from the Green River Formation, *Geology*, 38, 527-530,  
702 10.1130/g30630.1, 2010.  
703 Storey, M., Duncan, R. A., and Swisher, C. C., III: Paleocene-Eocene Thermal Maximum and the Opening  
704 of the Northeast Atlantic, *Science*, 316, 587-589, 10.1126/science.1135274, 2007.  
705 Suganuma, Y., and Ogg, J. G.: Campanian through Eocene magnetostratigraphy of Sites 1257–1261, ODP  
706 Leg 207, Demerara Rise (western equatorial Atlantic), in: Proc. ODP, Sci. Results, 207: College  
707 Station, TX (Ocean Drilling Program), edited by: Mosher, D. C., Erbacher, J., and Malone, M. J., 1-48,  
708 10.2973/odp.proc.sr.207.102.2006, 2006, Place: College Station, TX, Publisher: Ocean Drilling  
709 Program, Texas A&M University  
710 Tsukui, K., and Clyde, W. C.: Fine-tuning the calibration of the early to middle Eocene geomagnetic  
711 polarity time scale: Paleomagnetism of radioisotopically dated tuffs from Laramide foreland basins,  
712 *Geological Society of America Bulletin*, 124, 870-885, 10.1130/b30545.1, 2012.  
713 Vandenberghe, N., Hilgen, F. J., Speijer, R. P., Ogg, J. G., Gradstein, F. M., Hammer, O., Hollis, C. J., and  
714 Hooker, J. J.: Chapter 28 - The Paleogene Period, in: *The Geologic Time Scale*, edited by: Gradstein, F.  
715 M., Ogg, J. G., Schmitz, M. D., and Ogg, G. M., Elsevier, Boston, 855-921,  
716 <http://dx.doi.org/10.1016/B978-0-444-59425-9.00028-7>, 2012.  
717 Westerhold, T., Röhl, U., Laskar, J., Bowles, J., Raffi, I., Lourens, L. J., and Zachos, J. C.: On the duration  
718 of magnetochrons C24r and C25n and the timing of early Eocene global warming events: Implications  
719 from the Ocean Drilling Program Leg 208 Walvis Ridge depth transect, *Paleoceanography*, 22, PA2201,  
720 10.1029/2006PA001322, 2007.  
721 Westerhold, T., Röhl, U., Raffi, I., Fornaciari, E., Monechi, S., Reale, V., Bowles, J., and Evans, H. F.:  
722 Astronomical calibration of the Paleocene time, *Palaeogeography, Palaeoclimatology, Palaeoecology*,  
723 257, 377-403, 10.1016/j.palaeo.2007.09.016, 2008.  
724 Westerhold, T., and Röhl, U.: High resolution cyclostratigraphy of the early Eocene - new insights into the  
725 origin of the Cenozoic cooling trend, *Clim Past*, 5, 309-327, 10.5194/cp-5-309-2009, 2009.  
726 Westerhold, T., Röhl, U., McCarren, H. K., and Zachos, J. C.: Latest on the absolute age of the Paleocene-  
727 Eocene Thermal Maximum (PETM): New insights from exact stratigraphic position of key ash  
728 layers+19 and-17, *Earth and Planetary Science Letters*, 287, 412-419, 10.1016/j.epsl.2009.08.027, 2009.  
729 Westerhold, T., Röhl, U., and Laskar, J.: Time scale controversy: Accurate orbital calibration of the early  
730 Paleogene, *Geochem. Geophys. Geosyst.*, 13, Q06015, 10.1029/2012gc004096, 2012.  
731 Westerhold, T., and Röhl, U.: Orbital pacing of Eocene climate during the Middle Eocene Climate  
732 Optimum and the Chron C19r event: Missing link found in the tropical western Atlantic, *Geochemistry,  
733 Geophysics, Geosystems*, 14, 4811-4825, 10.1002/ggge.20293, 2013.  
734 Westerhold, T., Röhl, U., Pälike, H., Wilkens, R., Wilson, P. A., and Acton, G.: Orbitally tuned timescale  
735 and astronomical forcing in the middle Eocene to early Oligocene, *Clim. Past*, 10, 955-973, 10.5194/cp-  
736 10-955-2014, 2014.

737 Wotzlaw, J.-F., Bindeman, I. N., Schaltegger, U., Brooks, C. K., and Naslund, H. R.: High-resolution  
738 insights into episodes of crystallization, hydrothermal alteration and remelting in the Skaergaard  
739 intrusive complex, *Earth and Planetary Science Letters*, 355–356, 199-212, 10.1016/j.epsl.2012.08.043,  
740 2012.

741 Wotzlaw, J.-F., Schaltegger, U., Frick, D. A., Dungan, M. A., Gerdes, A., and Günther, D.: Tracking the  
742 evolution of large-volume silicic magma reservoirs from assembly to supereruption, *Geology*, 41, 867-  
743 870, 10.1130/g34366.1, 2013.

744 Wotzlaw, J.-F., Hüsing, S. K., Hilgen, F. J., and Schaltegger, U.: High-precision zircon U–Pb  
745 geochronology of astronomically dated volcanic ash beds from the Mediterranean Miocene, *Earth and*  
746 *Planetary Science Letters*, 407, 19-34, <http://dx.doi.org/10.1016/j.epsl.2014.09.025>, 2014.

747 Zachos, J. C., McCarren, H., Murphy, B., Röhl, U., and Westerhold, T.: Tempo and scale of late Paleocene  
748 and early Eocene carbon isotope cycles: Implications for the origin of hyperthermals, *Earth and*  
749 *Planetary Science Letters*, 299, 242-249, 10.1016/j.epsl.2010.09.004, 2010.

750 Zeeden, C., Rivera, T. A., and Storey, M.: An astronomical age for the Bishop Tuff and concordance with  
751 radioisotopic dates, *Geophysical Research Letters*, 41, 2014GL059899, 10.1002/2014GL059899, 2014.  
752

753 **Table 1.** Comparison of absolute magnetochron boundary ages in million years.

Magneto- chron	Standard GPTS			astronomically calibrated			astronomically calibrated – this study <sup>*</sup>		
	CK95	GPTS 2004	GPTS 2012	PEAT Sites <sup>#</sup>	Contessa Highway	ODP 1260 tuned	ODP 1258 option2	ODP 1263 tuned	ODP 702B tuned
<b>C18n.2n (o)</b>	40.130	39.464	40.145	<b>40.076 ±5</b>	41.120				
<b>C19n (y)</b>	41.257	40.439	41.154	<i>41.075 ±7</i>	41.250	<b>41.061 ±9</b>		41.030 ±13	
<b>C19n (o)</b>	41.521	40.671	41.390	<i>41.306 ±5</i>	41.510	<b>41.261 ±4</b>		41.180 ±11	
<b>C20n (y)</b>	42.536	41.590	42.301	<i>42.188 ±15</i>	42.540	<b>42.151 ±7</b>		42.107 ±13	42.124 ±4
<b>C20n (o)</b>	43.789	42.774	43.432		43.790	<b>43.449 ±18</b>		43.517 ±11	43.426 ±3
<b>C21n (y)</b>	46.264	45.346	45.724		46.310			<b>46.151 ±9</b>	46.080 ±3
<b>C21n (o)</b>	47.906	47.235	47.349				47.723 ±118	<b>47.575 ±18</b>	
<b>C22n (y)</b>	49.037	48.599	48.566					<b>48.954 ±16</b>	

754 <sup>\*</sup> tuned to the orbital solution La2011 (Laskar et al., 2011b)  
755 <sup>#</sup> combined ages based on Pacific Equatorial Age Transect Sites 1218, U1333 and U1334 (Westerhold et al., 2014)  
756 [Note: bold ages are the best estimates to be used for making a future reference time scale for polarity chrons](#)  
757

758

**Table 2.** Comparison of magnetostratigraphic boundary durations in million years.

Magneto- chron	Standard GPTS			astronomically calibrated			astronomically calibrated – this study <sup>*</sup>		
	CK95	GPTS 2004	GPTS 2012	PEAT Sites <sup>#</sup>	Contessa Highway	ODP 1260 tuned	ODP 1258 option2	ODP 1263 tuned	ODP 702B tuned
<b>C18n.2r</b>	1.127	0.975	1.009	0.999 ±12					
<b>C19n</b>	0.264	0.232	0.236	0.231 ±12	0.260	0.200 ±7		0.150 ±24	
<b>C19r</b>	1.015	0.919	0.911	0.882 ±20	1.030	0.891 ±6		0.927 ±24	
<b>C20n</b>	1.253	1.184	1.131		1.250	1.297 ±13		1.410 ±24	1.302 ±7
<b>C20r</b>	2.475	2.572	2.292		2.520			2.634 ±20	2.654 ±6
<b>C21n</b>	1.642	1.889	1.625					1.424 ±27	
<b>C21r</b>	1.131	1.364	1.214				1.231 ±134		

759  
760  
761<sup>\*</sup> tuned to the orbital solution La2011 (Laskar et al., 2011b)<sup>#</sup> combined ages based on Pacific Equatorial Age Transect Sites 1218, U1333 and U1334 (Westerhold et al., 2014)

762 **Table 3.** Astronomically calibrated ages of key events in the Eocene and Paleocene.

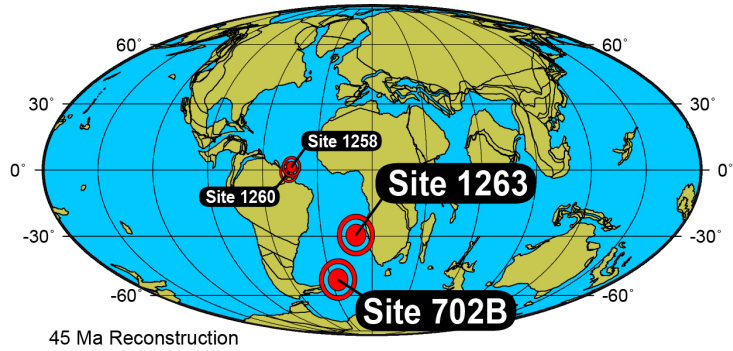
Event	Age (Ma)	Type	Source
<b>EOT</b>	33.89	Onset large scale glaciation of Antarctica	Westerhold et al. 2014
<b>peak-MECO CIE</b>	40.05	Hyperthermal	Westerhold & Röhl 2013
<b>C19r</b>	41.51	Hyperthermal	Westerhold & Röhl 2013
<b>X/K (ETM-3)</b>	52.83	Hyperthermal	Westerhold et al. 2012 Opt2
<b>ELMO (ETM-2)</b>	54.05	Hyperthermal	Westerhold et al. 2007 Opt2
<b>PETM (ETM-1)</b>	55.93	Hyperthermal	Westerhold et al. 2008 Opt2
<b>peak-PCIM event</b>	58.10	Shift in Pacific & Atlantic benthic carbon isotopes	Westerhold et al. 2008 Opt2
<b>ELPE (MPBE)</b>	59.27	Biotic turnover	Westerhold et al. 2008 Opt2
<b>LDE (Chron 27n)</b>	62.18	Hyperthermal	Dinarès-Turell et al. 2014
<b>Dan C2</b>	65.82 - 65.65	Hyperthermal	Dinarès-Turell et al. 2014
<b>K/Pg boundary</b>	66.022 ± 0.04	Impact	Dinarès-Turell et al. 2014

Note: Ages for the events from ELPE to X have been adjusted to La2011

763  
764  
765

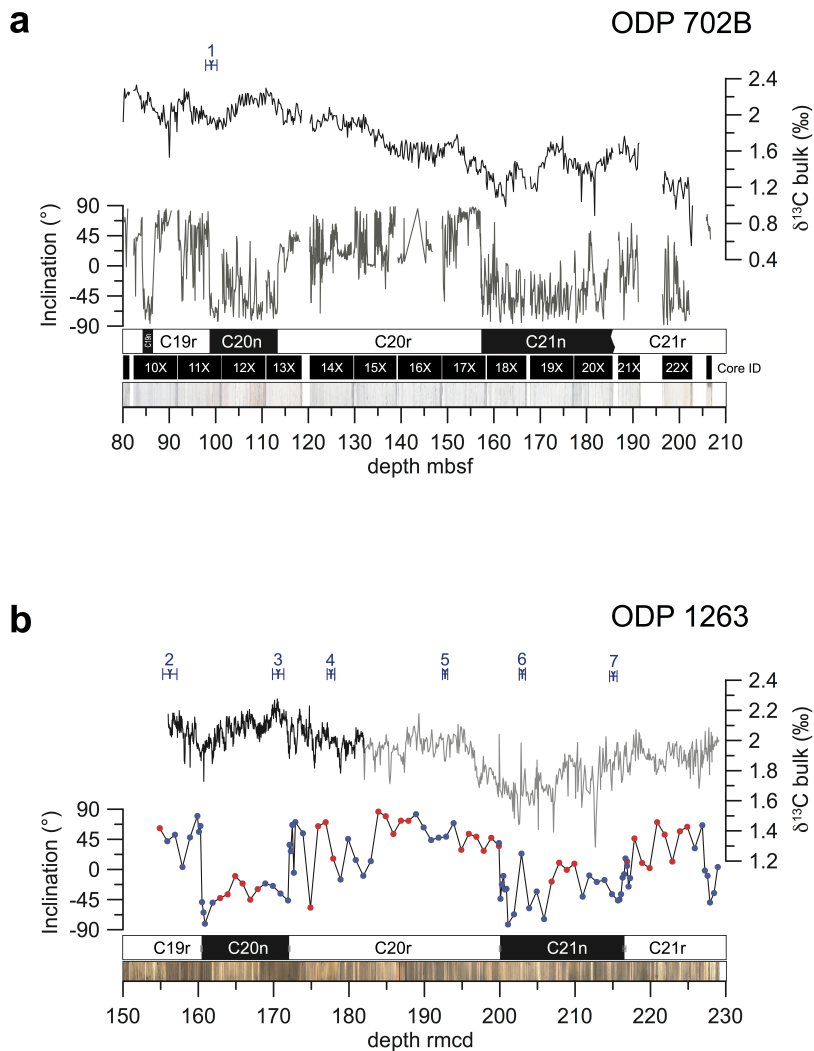
Autor  
Gelöscht: 02

767 **Figure Legends**

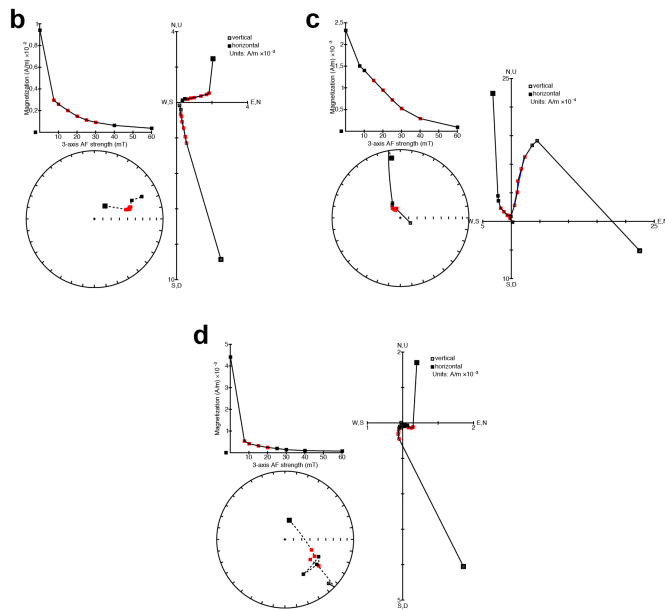
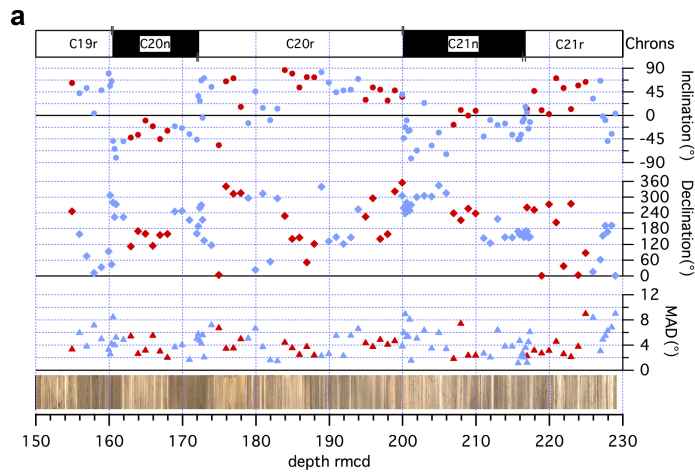


768

769 **Figure 1.** Location map for ODP Hole 702B and Site 1263 on a 45 Ma paleogeographic  
770 reconstruction in Mollweide projection (from <http://www.odsn.de>); also given location of  
771 ODP Sites 1258 and 1260.

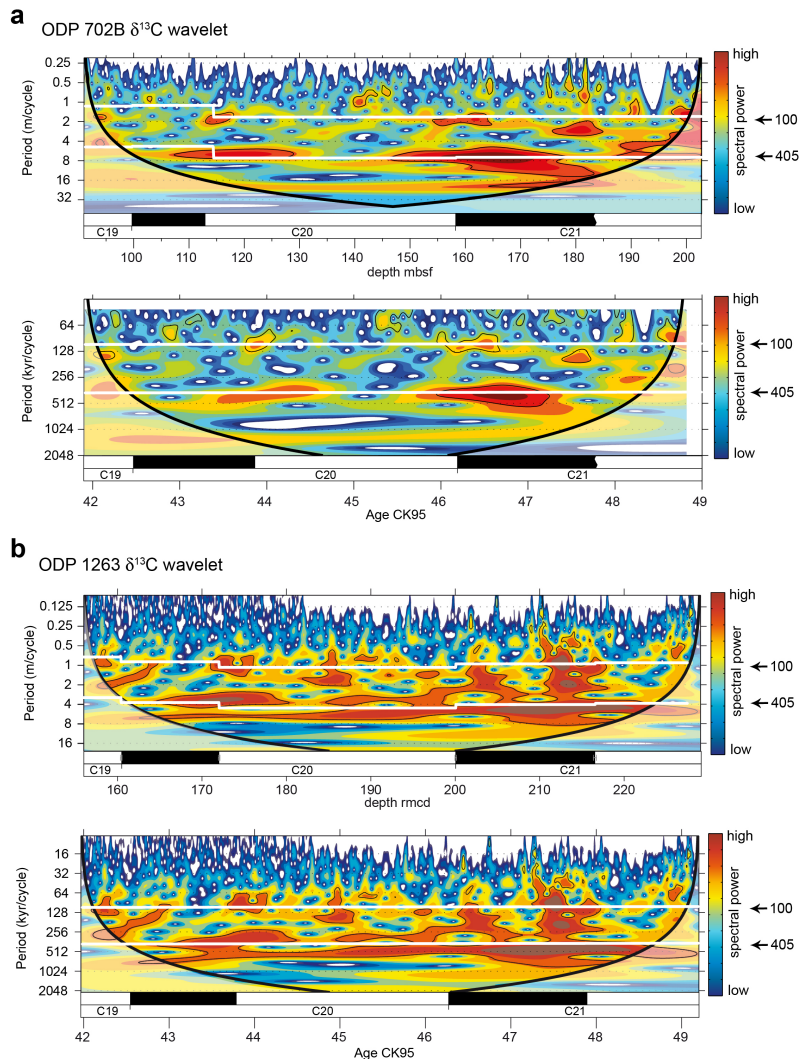


772  
 773 **Figure 2.** Overview of data from ODP Hole 702B and Site 1263 generated in this study.  
 774 **a.** bulk stable carbon (black) data generated by this study, inclination data (gray,  
 775 (Clement and Hailwood, 1991)), magnetostratigraphic interpretation, core ID and core  
 776 images vs. depth. **b.** ODP Site 1263 data generated by this study vs. revised composite  
 777 depth: bulk stable carbon isotope data (black Bremen lab, gray Santa Cruz lab),  
 778 inclination data (red dots 1263A, blue dots 1263B), magnetostratigraphic interpretation  
 779 and core images. Numbers with error bars mark calcareous nannofossil events (2, 4): 1.  
 780 Base *R. umbilicus* >14 $\mu\text{m}$ ., 2. Top *Nannotetrina* spp., 3. Top *N. fulgens*, 4. Top *C. gigas*,  
 781 5. Base *C. gigas*, 6. Base *N. fulgens*, 7. Top *D. lodoensis*.  
 782



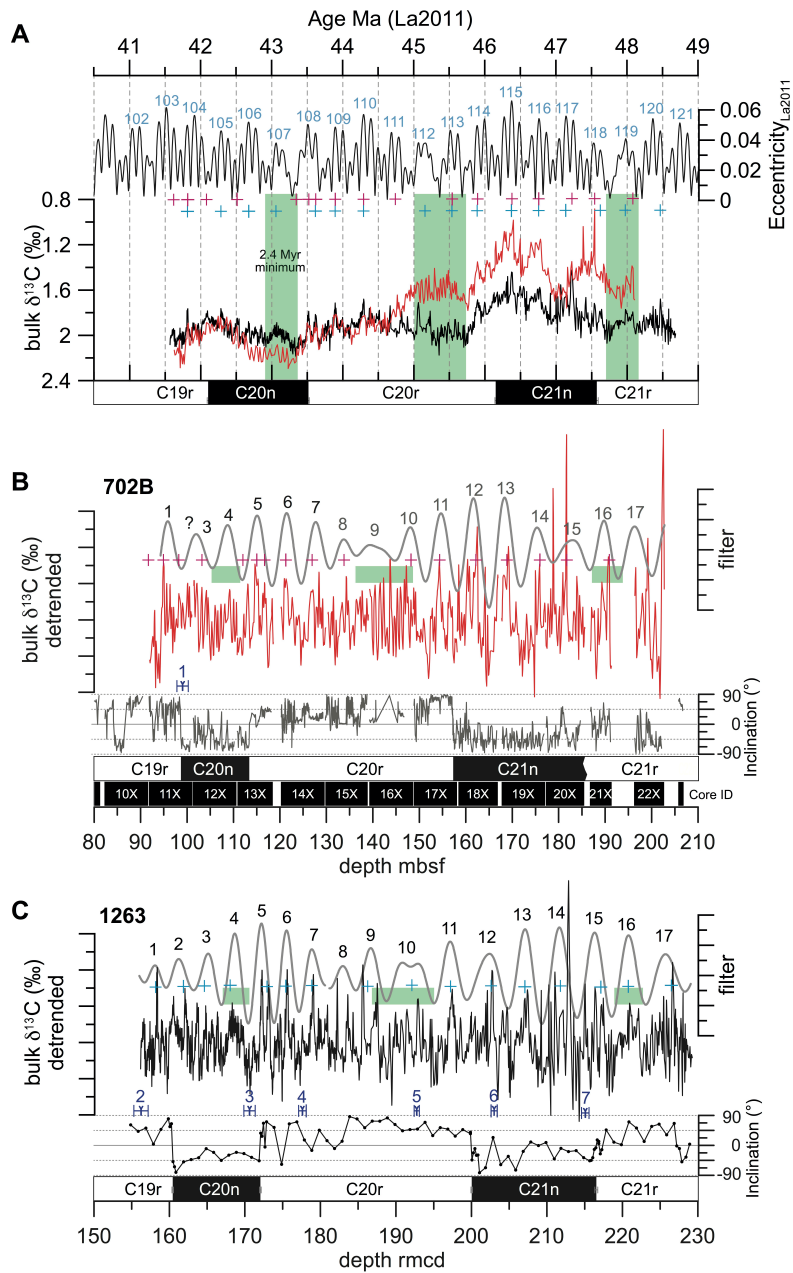
783

784 **Figure 3.** Magnetic property data and Zijderveld plots for ODP Site 1263. **a.** Inclination  
 785 (dots), declination (diamonds) and MAD (triangles) of Characteristic Remanent  
 786 Magnetization obtained from ODP 1263. Red = 1263A, blue = 1263B. **b to d.** Showcase  
 787 Zijderveld plots (z-plots) for samples from C19r 1263B10H1, 140 (b); C21n 1263B14H5,  
 788 77 (c); C21r 1263A21H6, 81 (d). Zijderveld plots were realized with PuffinPlot software  
 789 (Lurcock and Wilson, 2012). For discussion see text.



790

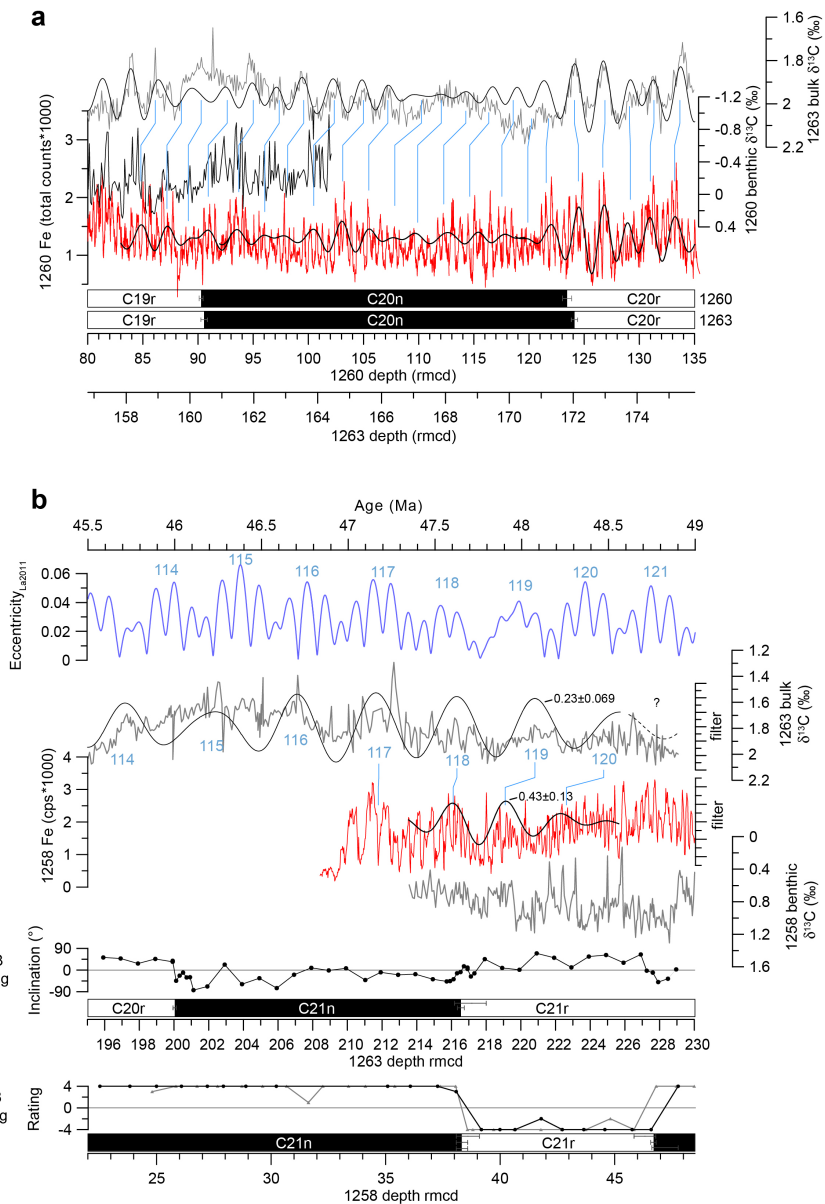
791 **Figure 4.** Evolutionary wavelet power spectra of bulk stable carbon isotope data from  
 792 ODP Hole 702B (A) and Site 1263 (B) for magnetochrons C19r to C21r in the depth  
 793 domain and versus age. The age model is based on magnetostratigraphy using the time  
 794 scale of Cande and Kent (1995, (Cande and Kent, 1995)). The shaded contours in the  
 795 evolutionary wavelet power spectra are normalized linear variiances with blue  
 796 representing low spectral power, and red representing high spectral power. The black  
 797 contour lines enclose regions with more than 95% confidence. Shaded regions on either  
 798 end indicate the cone of influence where edge effects become important. Distinct bands  
 799 that run across the spectra indicate the dominance of Milankovitch frequencies. Thick  
 800 white lines are the projected 100- and 405-kyr cycle path, respectively.



801

802 **Figure 5.** Middle Eocene cyclostratigraphic synthesis for ODP Sites 702 and 1263, 41–  
 803 48.5 Ma. (A) Orbital eccentricity solution La2011 (Laskar et al., 2011b) and respective  
 804 405-kyr cycle number with new astronomical calibrated ages for magnetic polarity chrons

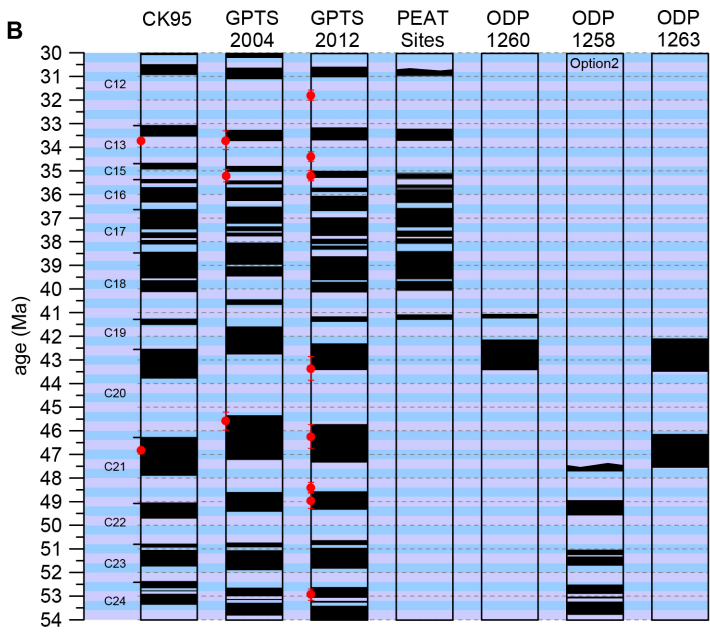
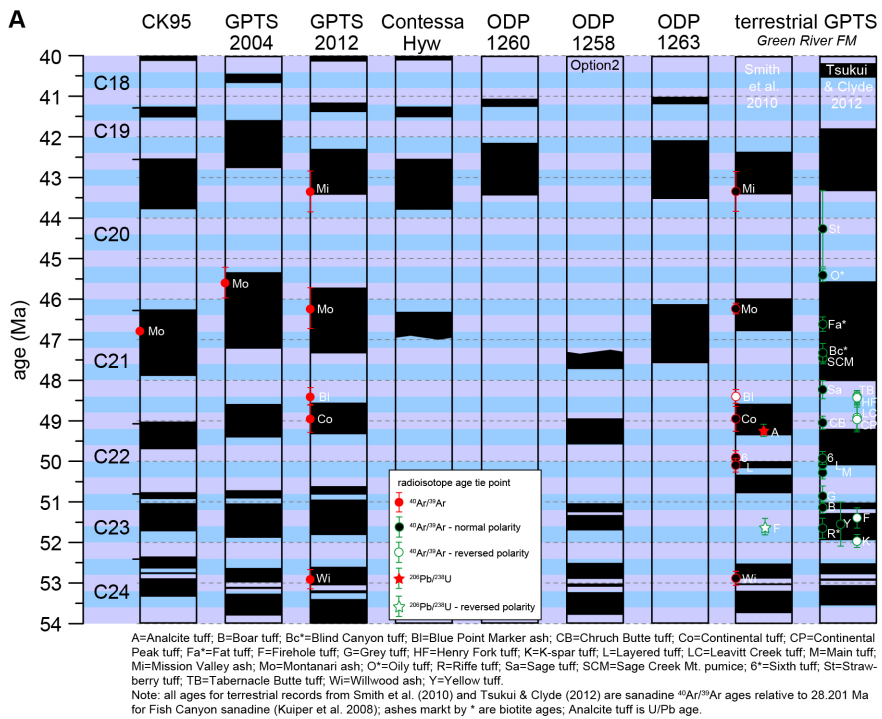
805 C20n, C20r and C21n. Bulk stable isotope data from Sites 702 (red) and 1263 (black) on  
806 the new astronomically tuned age model. Green bars show the minima in the amplitude  
807 modulation related to the 2.4-Myr cycle in eccentricity. (B) and (C) ODP Site 702 and  
808 1263 detrended bulk stable isotope data and band-pass filter of the 405-kyr related  
809 eccentricity component (Site 702:  $0.16 \pm 0.048$  cyc/m; Site 1263: 155–180 rmc  
810  $0.29 \pm 0.087$  cyc/m, 180–230 rmc  $0.23 \pm 0.069$  cyc/m), paleomagnetic inclination  
811 (Clement and Hailwood, 1991), calcareous nannofossil events (Pea, 2011; Shipboard  
812 Scientific Party, 2004), core recovery for Site 702. Black numbers indicate individual  
813 405-kyr cycles determined by combining records from both sites. Red and blue crosses  
814 indicate tuning tie points. Calcareous nannofossil events: 1. Base *R. umbilicus* >14 $\mu$ m, 2.  
815 Top *Nannotrinita* spp., 3. Top *N. fulgens*, 4. Top *C. gigas*, 5. Base *C. gigas*, 6. Base *N.*  
816 *fulgens*, 7. Top *D. lodoensis*.  
817



819

820 **Figure 6.** Connecting the 405-kyr cyclostratigraphy of ODP Sites 1258 and 1260 with  
 821 Site 1263. **A.** Correlation of geochemical and paleomagnetic data from ODP Sites 1263  
 822 and 1260. Site 1260: benthic  $\delta^{13}C$  in black (25), XRF core scanning Fe intensities in red

823 (5), magnetostratigraphy (Ogg and Bardot, 2001). Site 1263: Bulk  $\delta^{13}\text{C}$  data in gray,  
824 magnetostratigraphy (both this study). For  $\delta^{13}\text{C}$  and Fe data also the 100-kyr related cycle  
825 is filtered in the depth and age domain. Blue lines mark tie points between records. **B.**  
826 Tying ODP Site 1258 with the astronomically calibrated Site 1263 record at the  
827 magnetochron C21n/C21r boundary. From top to bottom: La2011 eccentricity solution;  
828 bulk  $\delta^{13}\text{C}$  data and 100-kyr filter from 1263 (this study); XRF core scanning Fe  
829 intensities (Westerhold and Röhl, 2009) and benthic  $\delta^{13}\text{C}$  data (Sexton et al., 2011) from  
830 1258; inclination data and magnetostratigraphic interpretation of 1263 (this study);  
831 polarity rating scheme and magnetostratigraphic interpretation of 1258 (Suganuma and  
832 Ogg, 2006; Westerhold and Röhl, 2009). The blue numbers label the 405-kyr cycle  
833 counted back in time from today in La2011 and the respective 405-kyr cycle in 1263. The  
834 small black numbers are the filter details for 1263  $\delta^{13}\text{C}$  and 1258 Fe. The correlation of  
835 cycle 118 and 119 over the magnetochron C21n/C21r boundary using  $\delta^{13}\text{C}$  data connects  
836 the cyclostratigraphy of the early Paleogene with the ATS of the Neogene and late  
837 Paleogene. This closes the mid-Eocene cyclostratigraphic gap and concludes a fully  
838 calibrated ATS for the entire Cenozoic.



840 **Figure 7.** Geomagnetic Polarity Time Scale of CK95 (Cande and Kent, 1995),  
841 GPTS2004 (Ogg and Smith, 2004) and GPTS2012 (Ogg, 2012; Vandenberghe et al.,  
842 2012) compared to astronomical calibrations of magnetochrons from Contessa Highway  
843 (Jovane et al., 2010), PEAT sites (Westerhold et al., 2014), Site 1260 (Westerhold and  
844 Röhl, 2013), Site 1258 (Westerhold and Röhl, 2009; Westerhold et al., 2012) and 1263  
845 (this study) from (A) 40-54 Ma and (B) 30-54 Ma. In (A) the terrestrial calibration of the  
846 GPTS from the Green River Formation (Smith et al., 2010; Tsukui & Clyde, 2012) is  
847 also shown. Small red dots with error bars mark the radio-isotopic calibration points used  
848 for CK95, GPTS2004, GPTS2012, and Smith et al. (2010); green circles show calibration  
849 points for the terrestrial sections used by Tsukui & Clyde (2012). The overview  
850 demonstrates the consistent Eocene coverage from 30-54 Ma by ODP and IODP (PEAT  
851 Sites) derived stratigraphic data, and the discrepancy to as well as in the terrestrial GPTS.  
852

Autor

**Gelöscht:** Small red dots with error bars mark the radio-isotopic calibration points used for CK95, GPTS2004 and GPTS2012.

Please find the marked changes to the supplement below

### **Expression of precession and short-eccentricity cycles in core images**

To illustrate the possible expression of precession and short-eccentricity cycles in core images we provide two figures on Sites 702 and 1263 core data. The hierarchical expression of cyclicity or bundling of cycles is easy to recognize in the Paleocene and Maastrichtian Zumaia section (Dinarès-Turell et al., 2003; Kuiper et al., 2008; Dinarès-Turell et al., 2013; Batenburg et al., 2014; Dinarès-Turell et al., 2014). Figure S4a displays the 166 to 180 rmcd interval at Site 1263 including a 2.4 Myr minimum at approximately 168 rmcd to a more pronounced short eccentricity cyclicity below. The figure shows the individual images from two holes, 1263A and 1263B, as well as the combined (spliced) image. Slight color differences between Holes 1263A and 1263B image are related to aperture setting changes during the shipboard image acquisition. These color differences between the two holes are artifacts that cannot easily be corrected for. There is no clear expression of precession although slight changes in color may occur on decimeter level. The short eccentricity cycles appear a bit darker at  $\delta^{13}\text{C}$  minima corresponding to eccentricity maxima, similar to the observations of Lourens et al. (2005) for the early Eocene. Core images of Hole 702B (Fig. S4b) are bright white with no apparent expressions of precession or short eccentricity cycles. The figure shows Cores 702B-12X and 702B-13X, time equivalents to the 1263 images of Fig. S4a. In general, core-box images taken during ODP times (“table layout images”) suffer from severe unequal lighting. Because of this most cores are darker in the upper right corner (see 702B-12X in Fig. S4b). Both ODP cores do not show the clear cycle bundling as in some outcrops on land (Zumaia) that can be utilized for astronomical tuning.

### **Phase relationship between bulk carbon isotopes and eccentricity**

For the astronomical tuning of the bulk  $\delta^{13}\text{C}$  data from 702B and 1263 lighter (more negative)  $\delta^{13}\text{C}$  peaks are correlated to La2011 eccentricity maxima. The rationale for picking this phase relationship is based on several high profile studies, including modeling of carbon cycle and Earth’s orbit interaction (Zachos et al., 2001a; Cramer et al., 2003; Billups et al., 2004; Lourens et al., 2005; Pälike et al., 2006a; Pälike et al., 2006b; Holbourn et al., 2007; Tian et al., 2008; Russon et al., 2010; Zachos et al., 2010; Lunt et al., 2011; Ma et al., 2011; Sexton et al., 2011; Westerhold et al., 2011; Proistosescu et al., 2012; Holbourn et al., 2013; Kirtland Turner et al., 2014; Littler et al., 2014) dealing with the phase relation of  $\delta^{13}\text{C}$  and the 405-kyr orbital eccentricity cycle. All these studies show that the Pliocene to Cenozoic  $\delta^{13}\text{C}$  values in benthic and bulk deep sea carbonate reveal augmented 405-kyr cycles with minima in  $\delta^{13}\text{C}$  (lighter values) and  $\%\text{CaCO}_3$  (i.e. peaks in Fe) corresponding to eccentricity

maxima. This phase relation is also observed in the records from ODP Site 1258 (Kirtland Turner et al., 2014) and 1260 (Edgar et al., 2007) as shown herein. The  $\delta^{13}\text{C}$  cycles are consistent with a climate-carbon cycle feedback, as indicated by a relative lag in  $\delta^{13}\text{C}$  relative to  $\delta^{18}\text{O}$ . [The strong 405-kyr cycle in benthic and bulk  \$\delta^{13}\text{C}\$  data as well as simulated  \$\delta^{13}\text{C}\$  results from a resonance associated with the long residence time of carbon in the ocean \(Broecker and Peng, 1982; Pälike et al., 2006a; Ma et al., 2011\). Periodic changes in oceanic  \$\delta^{13}\text{C}\$  on Milankovitch time scales are likely caused by changes in weathering induced carbon input changing the burial ratio of  \$\text{CaCO}\_3\$  to organic carbon \(Cramer et al., 2003; Ma et al., 2011\). An increase in weathering intensity and riverine carbon supply will increase the burial ratio of  \$\text{CaCO}\_3\$  to organic carbon leading to a decrease in  \$\delta^{13}\text{C}\$  \(minima, lighter values in bulk  \$\delta^{13}\text{C}\$ \). During eccentricity maxima weathering intensity and nutrient supply is enhanced leading via the biosphere productivity feedback to lighter bulk  \$\delta^{13}\text{C}\$  values in the stable carbon isotope records.](#) The phase lag of  $\delta^{13}\text{C}$  to eccentricity has been estimated to be in the order of 50 and 10 kyr for long and short eccentricity (Herbert, 1997; Zachos et al., 2001b; Holbourn et al., 2007; Zachos et al., 2010; Westerhold et al., 2011) in the Neogene and Paleogene. This leads to the assumption that the uncertainty in astronomical tuning presented here is in the order of less than 50 kyr. In fact the main uncertainty derives from the error in the 405-kyr eccentricity cycle in the order of 50 kyr at 56 Ma and 60 kyr at 66 Ma.

## References:

- Batenburg, S. J., Gale, A. S., Sprovieri, M., Hilgen, F. J., Thibault, N., Boussaha, M., and Orue-Etxebarria, X.: An astronomical time scale for the Maastrichtian based on the Zumaia and Sopelana sections (Basque country, northern Spain), *Journal of the Geological Society*, 10.1144/jgs2013-015, 2014.
- Billups, K., Pälike, H., Channell, J. E. T., Zachos, J. C., and Shackleton, N. J.: Astronomic calibration of the late Oligocene through early Miocene geomagnetic polarity time scale, *Earth and Planetary Science Letters*, 224, 33-44, 2004.
- Broecker, W. S., and Peng, T. H.: *Tracers in the Sea*, edited by: University, C., Lamont Doherty Geol. Obs. Publications, New York, 689 pp., 1982.
- Channell, J. E. T., Hodell, D. A., Singer, B. S., and Xuan, C.: Reconciling astrochronological and  $^{40}\text{Ar}/^{39}\text{Ar}$  ages for the Matuyama-Brunhes boundary and late Matuyama Chron, *Geochem. Geophys. Geosyst.*, 11, 21, 10.1029/2010GC003203 2010.
- Charles, A. J., Condon, D. J., Harding, I. C., Pälike, H., Marshall, J. E. A., Cui, Y., Kump, L., and Croudace, I. W.: Constraints on the numerical age of the Paleocene-Eocene boundary, *Geochem. Geophys. Geosyst.*, 12, Q0AA17, 10.1029/2010ge003426, 2011.
- Cramer, B. S., Wright, J. D., Kent, D. V., and Aubry, M.-P.: Orbital climate forcing of  $\delta^{13}\text{C}$  excursions in the late Paleocene - Eocene (chrons C24n-C25n), *Paleoceanography*, 18, 1097, 10.1029/2003PA000909, 2003.
- Dinarès-Turell, J., Baceta, J. I., Pujalte, V., Orue-Etxebarria, X., Bernaola, G., and Lorito, S.: Untangling the Paleocene climatic rhythm: an astronomically calibrated Early Paleocene magnetostratigraphy and biostratigraphy at Zumaia (Basque basin, northern Spain), *Earth and Planetary Science Letters*, 216, 483-500, 2003.
- Dinarès-Turell, J., Pujalte, V., Stoykova, K., and Elorza, J.: Detailed correlation and astronomical forcing within the Upper Maastrichtian succession in the Basque Basin, *Boletín Geológico y Minero*, 124, 253-282, 2013.
- Dinarès-Turell, J., Westerhold, T., Pujalte, V., Röhl, U., and Kroon, D.: Astronomical calibration of the Danian stage (Early Paleocene) revisited: Settling chronologies of sedimentary records across the Atlantic and Pacific Oceans, *Earth and Planetary Science Letters*, 405, 119-131, 10.1016/j.epsl.2014.08.027, 2014.
- Edgar, K. M., Wilson, P. A., Sexton, P. F., and Sugaanuma, Y.: No extreme bipolar glaciation during the main Eocene calcite compensation shift, *Nature*, 448, 908-911, 10.1038/nature06053, 2007.
- Herbert, T. D.: A long marine history of carbon cycle modulation by orbital-climatic changes, *Proc. Natl. Acad. Sci. USA*, 94, 8362-8369, 1997.
- Holbourn, A., Kuhnt, W., Schulz, M., Flores, J.-A., and Andersen, N.: Orbitally-paced climate evolution during the middle Miocene "Monterey" carbon-isotope excursion, *Earth and Planetary Science Letters*, 261, 534-550, 2007.
- Holbourn, A., Kuhnt, W., Clemens, S., Prell, W., and Andersen, N.: Middle to late Miocene stepwise climate cooling: Evidence from a high-resolution deep water isotope curve spanning 8 million years, *Paleoceanography*, 28, 2013PA002538, 10.1002/2013PA002538, 2013.

- Kirtland Turner, S., Sexton, P. F., Charles, C. D., and Norris, R. D.: Persistence of carbon release events through the peak of early Eocene global warmth, *Nature Geosci.*, 7, 10.1038/ngeo2240, 2014.
- Kuiper, K. F., Deino, A., Hilgen, F. J., Krijgsman, W., Renne, P. R., and Wijbrans, J. R.: Synchronizing Rock Clocks of Earth History, *Science*, 320, 500-504, 10.1126/science.1154339, 2008.
- Laskar, J., Fienga, A., Gastineau, M., and Manche, H.: La2010: a new orbital solution for the long-term motion of the Earth, *Astronomy and Astrophysics*, 532, A89, 10.1051/0004-6361/201116836, 2011a.
- Laskar, J., Gastineau, M., Delisle, J. B., Farrés, A., and Fienga, A.: Strong chaos induced by close encounters with Ceres and Vesta, *Astronomy and Astrophysics*, 532, L4, 10.1051/0004-6361/201117504, 2011b.
- Littler, K., Röhl, U., Westerhold, T., and Zachos, J. C.: A high-resolution benthic stable-isotope record for the South Atlantic: Implications for orbital-scale changes in Late Paleocene–Early Eocene climate and carbon cycling, *Earth and Planetary Science Letters*, 401, 18-30, 10.1016/j.epsl.2014.05.054, 2014.
- Lourens, L. J., Sluijs, A., Kroon, D., Zachos, J. C., Thomas, E., Röhl, U., Bowles, J., and Raffi, I.: Astronomical pacing of late Palaeocene to early Eocene global warming events, *Nature*, 435, 1083-1087, 10.1038/nature03814, 2005.
- Lunt, D. J., Ridgwell, A., Sluijs, A., Zachos, J., Hunter, S., and Haywood, A.: A model for orbital pacing of methane hydrate destabilization during the Palaeogene, *Nature Geosci.*, 4, 775-778, 10.1038/ngeo1266, 2011.
- Ma, W., Tian, J., Li, Q., and Wang, P.: Simulation of long eccentricity (400-kyr) cycle in ocean carbon reservoir during Miocene Climate Optimum: Weathering and nutrient response to orbital change, *Geophysical Research Letters*, 38, L10701, 10.1029/2011GL047680, 2011.
- Pälike, H., Frazier, J., and Zachos, J. C.: Extended orbitally forced palaeoclimatic records from the equatorial Atlantic Ceara Rise, *Quaternary Science Reviews*, 25, 3138-3149, 2006a.
- Pälike, H., Norris, R. D., Herrle, J. O., Wilson, P. A., Coxall, H. K., Lear, C. H., Shackleton, N. J., Tripati, A. K., and Wade, B. S.: The Heartbeat of the Oligocene Climate System, *Science*, 314, 1894-1898, 10.1126/science.1133822, 2006b.
- Proistosescu, C., Huybers, P., and Maloof, A. C.: To tune or not to tune: Detecting orbital variability in Oligo-Miocene climate records, *Earth and Planetary Science Letters*, 325-326, 100-107, 10.1016/j.epsl.2012.01.022, 2012.
- Renne, P. R., Swisher, C. C., Deino, A. L., Karner, D. B., Owens, T. L., and DePaolo, D. J.: Intercalibration of standards, absolute ages and uncertainties in  $^{40}\text{Ar}/^{39}\text{Ar}$  dating, *Chemical Geology*, 145, 117-152, 1998.
- Renne, P. R., Mundil, R., Balco, G., Min, K., and Ludwig, K. R.: Joint determination of  $^{40}\text{K}$  decay constants and  $^{40}\text{Ar}/^{40}\text{K}$  for the Fish Canyon sanidine standard, and improved accuracy for  $^{40}\text{Ar}/^{39}\text{Ar}$  geochronology, *Geochimica et Cosmochimica Acta*, 74, 5349-5367, 10.1016/j.gca.2010.06.017, 2010.
- Rivera, T. A., Storey, M., Zeeden, C., Hilgen, F. J., and Kuiper, K.: A refined astronomically calibrated  $^{40}\text{Ar}/^{39}\text{Ar}$  age for Fish Canyon sanidine, *Earth and Planetary Science Letters*, 311, 420-426, 10.1016/j.epsl.2011.09.017, 2011.
- Russon, T., Paillard, D., and Elliot, M.: Potential origins of 400–500 kyr periodicities in the ocean carbon cycle: A box model approach, *Global Biogeochemical Cycles*, 24, GB2013, 10.1029/2009GB003586, 2010.
- Sexton, P. F., Norris, R. D., Wilson, P. A., Pälike, H., Westerhold, T., Röhl, U., Bolton, C. T., and Gibbs, S.: Eocene global warming events driven by ventilation of oceanic dissolved organic carbon, *Nature*, 471, 349-352, 10.1038/nature09826, 2011.
- Shipboard Scientific Party: Site 1263, in: Proc. ODP. Init. Repts., 208: College Station, TX (Ocean Drilling Program), edited by: Zachos, J. C., Kroon, D., Blum, P., and et al., 1-87, 10.2973/odp.proc.ir.208.104.2004, 2004.
- Tian, J., Zhao, Q., Wang, P., Li, Q., and Cheng, X.: Astronomically modulated Neogene sediment records from the South China Sea, *Paleoceanography*, 23, 10.1029/2007PA001552, 2008.
- Westerhold, T., Röhl, U., Laskar, J., Bowles, J., Raffi, I., Lourens, L. J., and Zachos, J. C.: On the duration of magnetochrons C24r and C25n and the timing of early Eocene global warming events: Implications from the Ocean Drilling Program Leg 208 Walvis Ridge depth transect, *Paleoceanography*, 22, 10.1029/2006PA001322, 2007.
- Westerhold, T., Röhl, U., Raffi, I., Fornaciari, E., Monechi, S., Reale, V., Bowles, J., and Evans, H. F.: Astronomical calibration of the Paleocene time, *Paleogeography, Palaeoclimatology, Palaeoecology*, 257, 377-403, 10.1016/j.palaeo.2007.09.016, 2008.
- Westerhold, T., and Röhl, U.: High resolution cyclostratigraphy of the early Eocene - new insights into the origin of the Cenozoic cooling trend, *Clim Past*, 5, 309-327, 10.5194/cp-5-309-2009, 2009.
- Westerhold, T., Röhl, U., McCarren, H. K., and Zachos, J. C.: Latest on the absolute age of the Paleocene-Eocene Thermal Maximum (PETM): New insights from exact stratigraphic position of key ash layers+19 and -17, *Earth and Planetary Science Letters*, 287, 412-419, 10.1016/j.epsl.2009.08.027, 2009.
- Westerhold, T., Röhl, U., Donner, B., McCarren, H. K., and Zachos, J. C.: A complete high-resolution Paleocene benthic stable isotope record for the central Pacific (ODP Site 1209), *Paleoceanography*, 26, PA2216, 10.1029/2010pa002092, 2011.
- Westerhold, T., Röhl, U., and Laskar, J.: Time scale controversy: Accurate orbital calibration of the early Paleogene, *Geochem. Geophys. Geosyst.*, 13, Q06015, 10.1029/2012gc004096, 2012.
- Zachos, J., Pagani, M., Sloan, L., Thomas, E., and Billups, K.: Trends, Rhythms, and Aberrations in Global Climate 65 Ma to Present, *Science*, 292, 686-693, 10.1126/science.1059412, 2001a.
- Zachos, J., Shackleton, N. J., Revenaugh, J. S., Pälike, H., and Flower, B. P.: Climate Response to Orbital Forcing Across the Oligocene-Miocene Boundary, *Science*, 292, 274-278, 10.1126/science.1058288, 2001b.
- Zachos, J. C., McCarren, H., Murphy, B., Röhl, U., and Westerhold, T.: Tempo and scale of late Paleocene and early Eocene carbon isotope cycles: Implications for the origin of hyperthermals, *Earth and Planetary Science Letters*, 299, 242-249, 10.1016/j.epsl.2010.09.004, 2010.

## Figure Legends

**Figure S1.** ODP Site 1263 magnetic susceptibility data (Shipboard Scientific Party, 2004) from Holes A (red), B (blue) and C (green) on the new revised composite depth. Data and core images are plotted for each hole separately. Red vertical lines are the tops and yellow vertical lines are the bases of splice sections. All magnetic susceptibility data are the instrument units raw in  $10^{-5}$ .

Autor  
Gelöscht: of

**Figure S2.** MTM power spectra of ODP Hole 702B bulk  $\delta^{13}\text{C}$  data from various intervals in the depth and age (magnetostratigraphy ages CK95) domain.

**Figure S3.** MTM power spectra of ODP Site 1263 bulk  $\delta^{13}\text{C}$  data from various intervals in the depth and age (magnetostratigraphy ages CK95) domain.

**Figure S4.** Close up of ODP Site 1263 and Hole 702B to illustrate the potential expression of precession and short-eccentricity cycles in core images.

**Figure S5.** Comparison of sedimentation rates for Site 1263 and Hole 702B records using the tuned, the magnetostratigraphic, the 17 405-kyr cyclo- and 18 405-kyr cyclostratigraphic age model. Bulk  $\delta^{13}\text{C}$  data (gray) and the magnetostratigraphy are also shown.

**Figure S6.** Eccentricity solutions La2010a-d (Laskar et al., 2011a) and La2011 (Laskar et al., 2011b) of the Earth (fine black line) compared to geological data to assess the positions of the 2.4 myr eccentricity cycle minima from 41 to 60 Ma. To accentuate successive minima in the eccentricity solution the amplitude modulation (AM) was extracted from the orbital solution (thick gray line). Geochemical data with a dominant eccentricity component are plotted on the stable 405-kyr cyclostratigraphic framework anchored to the ATS. Data: bulk  $\delta^{13}\text{C}$  from 1258 in light blue (Kirtland Turner et al., 2014), 1262 in bright blue (Littler et al., 2014; Zachos et al., 2010) and 1263 in dark blue (this study); benthic  $\delta^{13}\text{C}$  from 1258 in gray (Sexton et al., 2011); XRF core scanning iron (Fe) intensity data from 1262 in orange (Westerhold et al., 2007; Westerhold et al., 2008) and 1258 in red (Westerhold and Röhl, 2009). Also given is the position of the Paleocene-Eocene Thermal Maximum (PETM) (Westerhold et al., 2007) and ash -17 (Westerhold et al., 2009). Light blue bars mark the 2.4 myr eccentricity minima in the geological data. The comparison shows that none of the orbital solutions matches all of the minima in the geological records back to 60 Ma. La2011 and La2010d reproduce all minima up to 48 Ma. Therefore, for astronomical dating only these two solutions are robust back to 48 Ma. For older times only the stable 405-kyr eccentricity cycle should be utilized.

**Figure S7.** Comparison of astronomical and radio-isotopic ages for the Paleocene-Eocene Thermal Maximum (PETM) and ash -17. Gray bars mark the absolute age range for the onset of the PETM based on the age and relative distance of ash -17 with respect to the age of the Fish Canyon (FC) radiometric dating  $^{40}\text{Ar}/^{39}\text{Ar}$  standard of 28.02 (Renne et al., 1998), 28.201 (Kuiper et al., 2008), 28.305 (Renne et al., 2010), 27.93 (Channell et al., 2010), 27.89 (Westerhold et al., 2012), 28.172 (Rivera et al., 2011) and 28.10 (this study) Ma. Horizontal black lines mark the three possible options of the age range for the onset of the PETM based on the astronomically calibrated Paleocene time scale (Westerhold et al., 2008). The red bar and arrow as well as light blue bar and arrow mark the astronomically calibrated absolute age for the onset of the PETM and ash -17 consistent with the 2.4 myr minima in the La2011 orbital solution (Westerhold et al., 2012). The green bar and arrow as well as the blue bar and arrow mark the age of the onset of the PETM and ash -17 consistent with the stable 405-kyr cyclostratigraphy established in this study. The black double dot with error bar shows the age of the onset of the PETM based on a high precision radio-isotopic U/Pb age of 55.728 - 55.964 Ma from bentonite layers within the PETM interval at Spitzbergen (Charles et al., 2011). The U/Pb age and the stable 405-kyr cyclostratigraphy age of ~55.9 Ma are independent from uncertainties in the 100-kyr and 2.4 myr eccentricity cycle components and therefore the most robust age for the onset of the PETM.

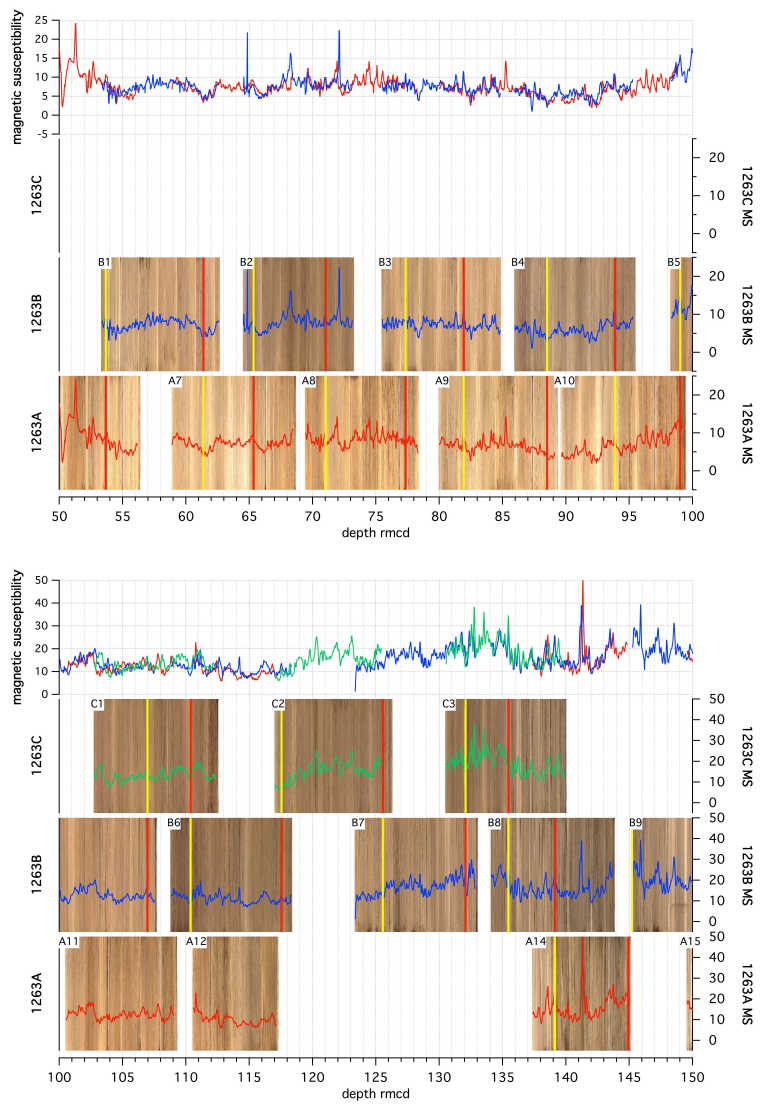


**Figure S1**

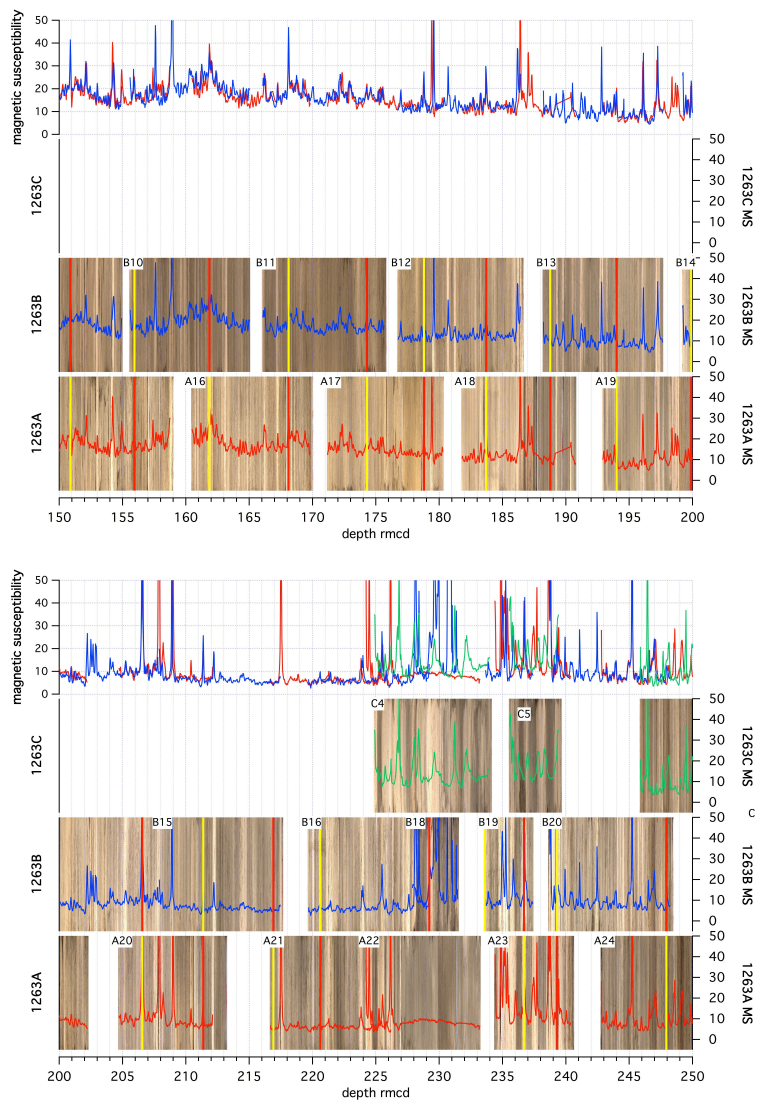


Figure S1 - continued.

702B bulk  $\delta^{13}\text{C}$

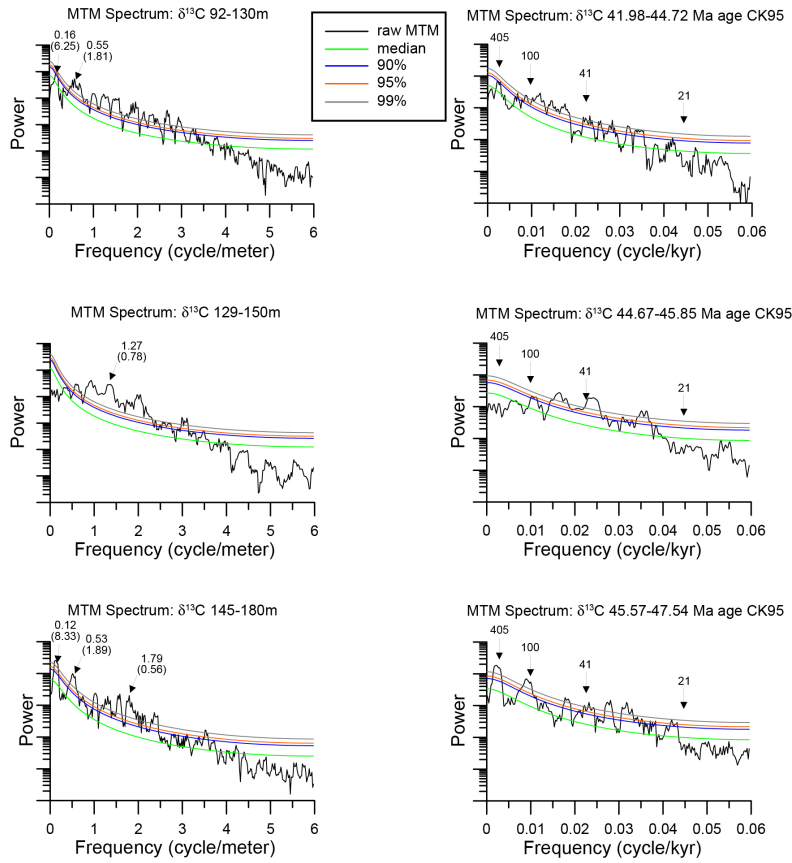


Figure S2

1263 bulk  $\delta^{13}\text{C}$

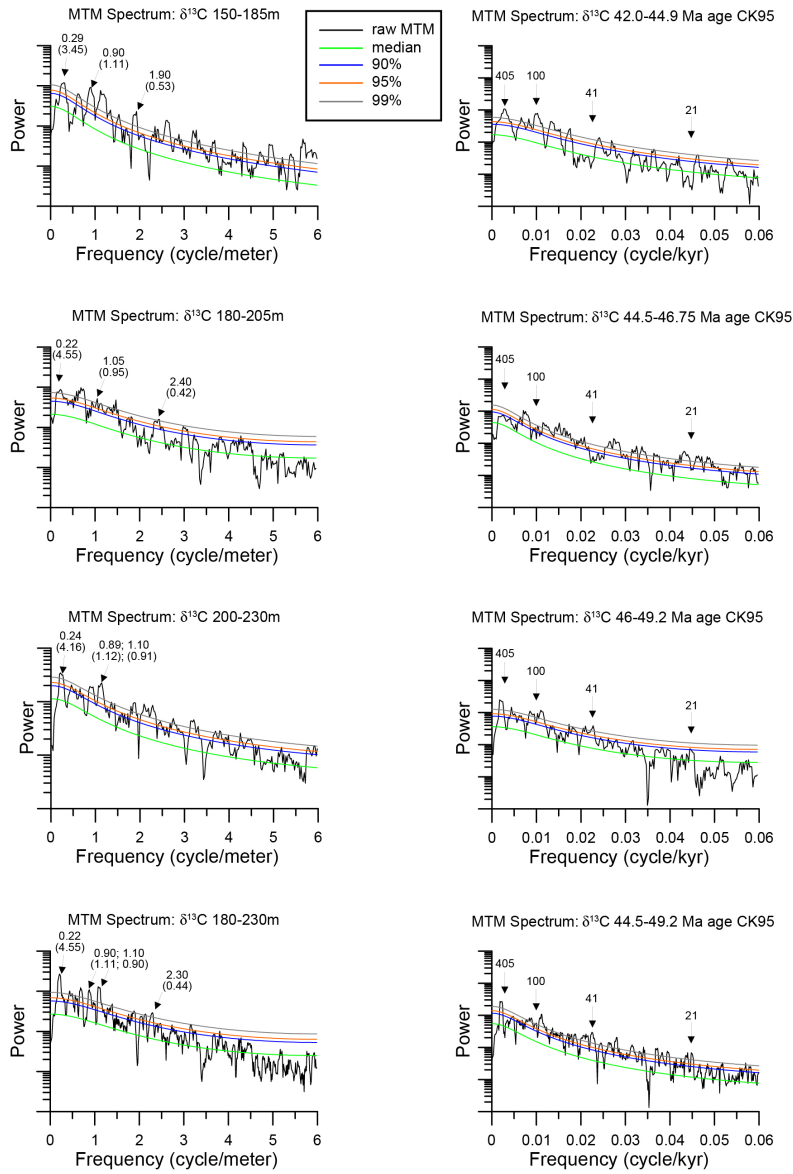
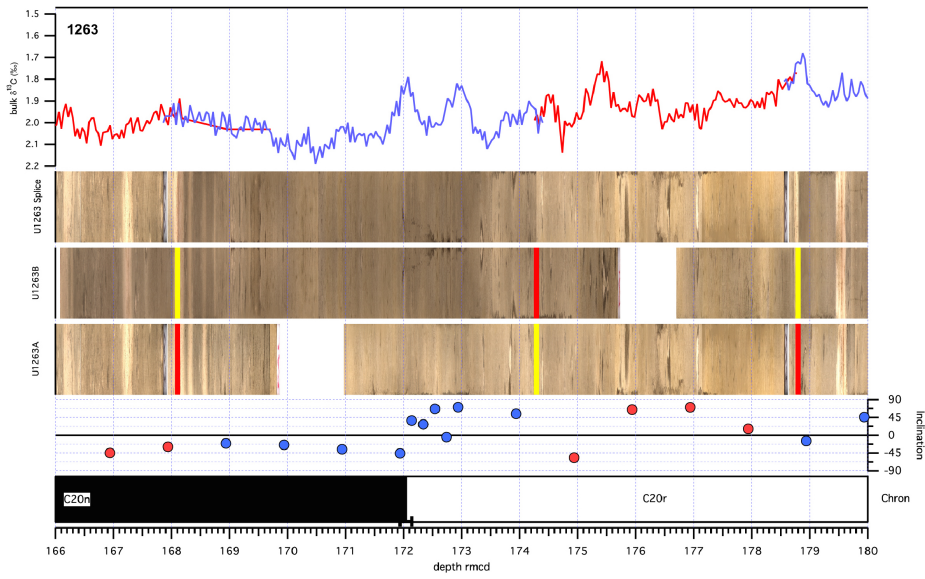


Figure S3

**a,**



**b,**

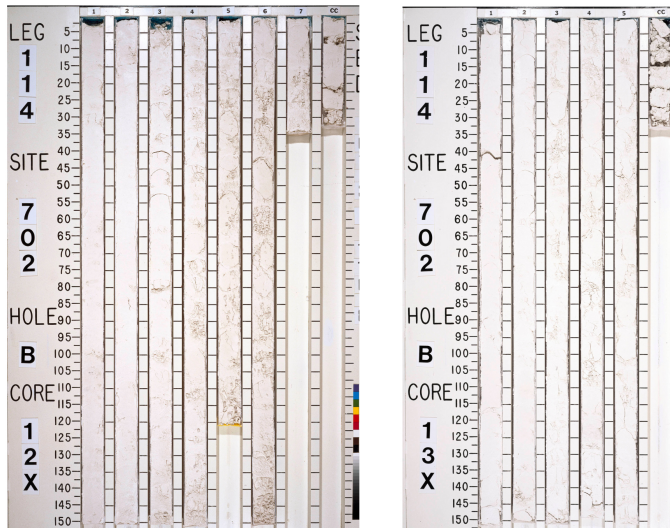


Figure S4

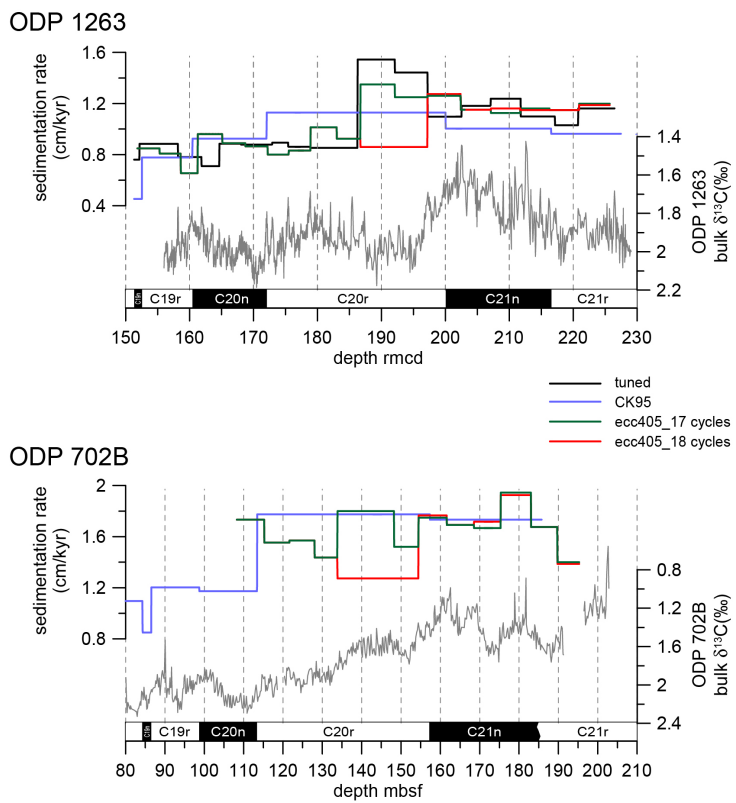


Figure S5

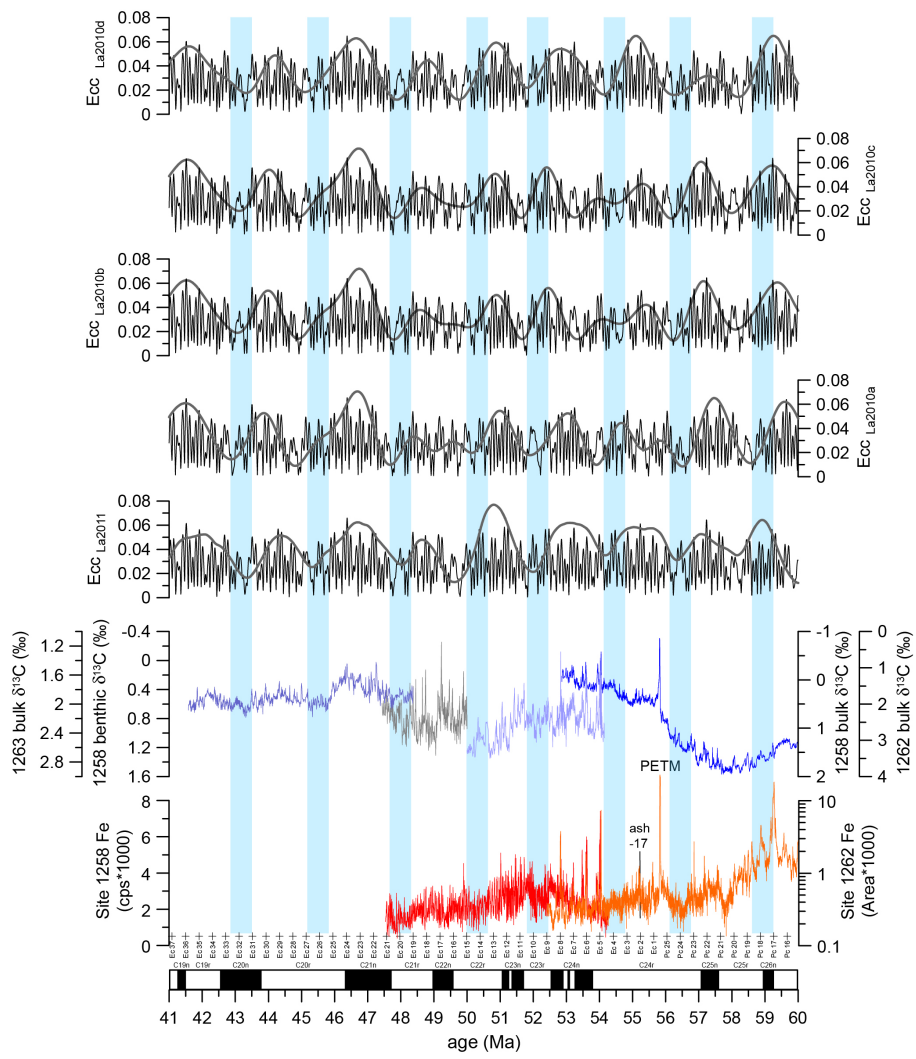


Figure S6

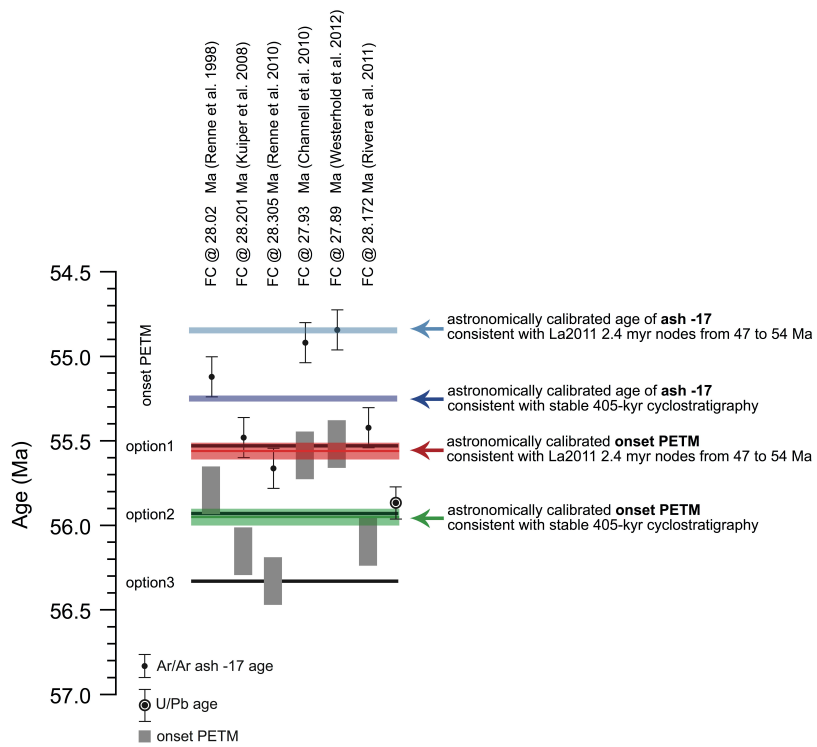


Figure S7

## Dataset

### Astronomical Calibration of the Geological Timescale: Closing the Middle Eocene Gap

Thomas Westerhold\*, Ursula Röhl, Thomas Frederichs, Steve M. Bohaty, James C. Zachos

\*email: [twesterhold@marum.de](mailto:twesterhold@marum.de)

The data reported in this paper are open access archived at the Pangaea ([www.pangaea.de](http://www.pangaea.de)) database online at <http://doi.pangaea.de/10.1594/PANGAEA.845986>. This supplement includes tables S4 to S13; extensive tables S1 to S3 are open access available at the links to Pangaea database.

#### Tables:

[Table S1 - Bulk stable isotope data ODP 702B \(available here\)](#)

[Table S2 - Bulk stable isotope data ODP 1263 \(available here\)](#)

[Table S3 – ODP 1263 raw inclination, declination, and intensity data for each measurement step \(available here\)](#)

[Table S4 - Magnetostratigraphy ODP 1263](#)

[Table S5 - Hole 702B and Site 1263 Calcareous Nannofossil datums](#)

[Table S6 - Relative and absolute 405-kyr eccentricity cycle age model for ODP Hole 702B and Site 1263](#)

[Table S7 - Offsets applied to cores from Holes 1263A, 1263B, 1263C](#)

[Table S8 - List of tie points to create the revised composite depth scale \(rmcd\) for Site 1263](#)

[Table S9 - Paleomagnetic data from ODP 1263](#)

[Table S10 - Astronomical tuning age tie points](#)

[Table S11 - Comparison of magnetochron boundary ages in million years](#)

[Table S12 - Comparison of magnetochron boundary durations in million years](#)

[Table S13 - Comparison of durations of magnetochrons in million years including uncertainties in magnetic anomaly width](#)

**Table S4** Magnetostratigraphy ODP 1263

Chron	Top			Bottom			Mean		
	Site, Hole, Core,	Depth		Site, Hole, Core,	Depth		Depth		Error
	Section, Interval (cm)	(mbsf)	(rmcd)	Section, Interval (cm)	(mbsf)	(rmcd)	(mbsf)	(rmcd)	(m)
C20n (y)	1263B-10H-4, 30	136.30	160.34	1263B-10H-4, 50	136.50	160.54	136.40	160.44	± 0.1
C20n (o)	1263B-11H-4, 141	146.91	171.94	1263B-11H-5, 11	147.11	172.14	147.01	172.04	± 0.1
C21n (y)	1263A-19H-5, 108	170.88	199.94	1263B-14H-1, 97	170.47	200.14	170.68	200.04	± 0.1
C21n (o)	1263B-15H-6, 99	185.49	216.34	1263B-15H-6, 39	185.89	216.74	185.69	216.54	± 0.2

**Table S5** Hole 702B and Site 1263 Calcareous Nannofossil datums

Bioevent	Age <sup>3</sup>	Position in <sup>4</sup>	Top		Bottom		Mean		error
			Core, section	interval (cm)	Core, section	interval (cm)	Depth	Depth	
		Magneto-							
		stratigraphy							(±m)
<b>Hole 702B<sup>5</sup></b>									
LO <i>R. umbilicus</i> >14µm	43.06	C20n.58	702B11X-5,5	702B11X-5,45	97.85	98.25	98.05	0.20	
<b>Site 1263<sup>6,7</sup></b>									
HO <i>Nannotetrina</i> spp.	43.06	C20n.58	1263A15H-CC	1263A16H-1,45	155.27	157.16	156.22	0.94	
HO <i>N. fulgens (alata)</i>	43.72	C20n	1263A15H-CC	1263B11H-4,80	169.84	171.34	170.59	0.75	
HO <i>C. gigas</i>	43.96	C20r.93	1263B12H-1,40	1263B12H-1,140	177.09	178.09	177.59	0.50	
LO <i>C. gigas</i>	46.11	C20r.06	1263B13H-3,120	1263B13H-4,40	192.38	193.08	192.73	0.35	
LO <i>N. fulgens (alata)</i>	46.80	C21n.68	1263B14H-3,40	1263B14H-3,120	202.58	203.39	202.99	0.40	
HO <i>D. lodoensis</i>	48.37	C21r.59	1263A21H-2,40	1263A21H-2,140	215.04	215.56	215.06	0.26	

Note: HO = highest occurrence, LO = lowest occurrence; <sup>3</sup>Agnini et al. 2014, <sup>4</sup>Pea 2011, <sup>5</sup>Shipboard Scientific Party 2004, <sup>6</sup>Position in Magnetochron is from Base of Chron; depth in 702B is mbsf and 1263 is rmcd.

**Table S6** Relative and absolute 405-kyr eccentricity cycle age model for ODP Hole 702B and Site 1263

405-kyr cycle	Site 702B	Site 1263	relative age (Ma)	absolute age	
	depth (mbsf)	depth (rmcd)		405-kyr cycle	La2011 (Ma)
# 1	-	158.60	0.405	# 104	41.904
# 2	-	161.25	0.810	# 105	42.308
# 3	-	165.10	1.215	# 106	42.708
# 4	108.20	168.70	1.620	# 107	43.112
# 5	115.20	172.20	2.025	# 108	43.516
# 6	121.60	175.50	2.430	# 109	43.928
# 7	128.00	178.90	2.835	# 110	44.336
# 8	133.80	183.00	3.240	# 111	44.740
# 9	-	186.70	3.645	# 112	45.140
# 10	148.20	(192.10)	4.050	# 113	45.540
# 11	154.40	197.20	4.455	# 114	45.948
# 12	161.60	202.40	4.860	# 115	46.360
# 13	168.50	207.10	5.265	# 116	46.768
# 14	175.30	211.70	5.670	# 117	47.176
# 15	183.00	216.30	6.075	# 118	47.572
# 16	189.70	220.90	6.480	# 119	47.972
# 17	195.30	225.70	6.885	# 120	48.372

**Table S7** Offsets applied to cores from Holes 1263A, 1263B, 1263C

Core	Offset Ship (m)	Revised Offset (m)	Δ Ship – Revised (m)	Depth		Source
				(mbsf)	(rmcd)	
<b>208-1263A-</b>						
1H	0.00	0.00	0.00	0.00	0.00	ship
2H	0.41	0.41	0.00	2.30	2.71	ship
3H	2.12	2.12	0.00	11.80	13.92	ship
4H	3.83	3.83	0.00	21.30	25.13	ship
5H	3.85	3.85	0.00	30.80	34.65	ship
6H	7.25	7.25	0.00	40.30	47.55	ship
7H	9.11	9.06	0.05	49.80	58.86	this study
8H	10.71	10.11	0.60	59.30	69.41	this study
9H	11.77	11.14	0.63	68.80	79.94	this study
10H	11.79	11.29	0.50	78.30	89.59	this study
11H	13.17	12.67	0.50	87.80	100.47	this study
12H	13.73	13.23	0.50	97.30	110.53	this study
13H	17.53	17.03	0.50	106.80	123.83	this study
14H	17.75	21.03	-3.28	116.30	137.33	this study
15H	20.52	23.73	-3.21	125.80	149.53	this study
16H	21.89	25.13	-3.24	135.30	160.43	this study
17H	23.02	26.34	-3.32	144.80	171.14	this study
18H	23.94	27.44	-3.50	154.30	181.74	this study
19H	25.47	29.06	-3.59	163.80	192.86	this study
20H	27.77	31.36	-3.59	173.30	204.66	this study
21H	30.34	33.83	-3.49	182.80	216.63	this study
22H*	32.34	31.86	0.48	192.30	224.16	this study
23H	32.55	32.55	0.00	201.80	234.35	ship
24H	34.65	34.65	0.00	208.10	242.75	ship
25H	35.85	35.85	0.00	217.60	253.45	ship
26H	36.85	36.85	0.00	222.60	259.45	ship
27H	40.03	40.03	0.00	232.10	272.13	ship
28H	42.52	42.52	0.00	241.60	284.12	ship
29H	43.70	43.78	-0.08	251.10	294.88	W07
30H	45.71	45.79	-0.08	260.60	306.39	W07
31H	46.40	46.48	-0.08	270.10	316.58	W07
32H	48.38	49.08	-0.70	271.60	320.68	W07
33H	51.00	50.60	0.40	281.10	331.70	W07
34X	51.24	50.86	0.38	284.10	334.96	W07
35X	52.36	51.98	0.38	290.30	342.28	W07
36X	54.10	53.72	0.38	300.00	353.72	W07
37X	55.38	55.00	0.38	307.10	362.10	W07
38X	57.11	56.73	0.38	316.70	373.43	W07
39X	58.85	58.47	0.38	326.40	384.87	W07
40X	60.58	60.20	0.38	336.00	396.20	W07
<b>208-1263B-</b>						
1H	7.31	7.30	0.01	46.00	53.30	this study
2H	9.41	9.00	0.41	55.50	64.50	this study
3H	11.04	10.45	0.59	65.00	75.45	this study
4H	12.09	11.43	0.66	74.50	85.93	this study
5H	14.69	14.25	0.44	84.00	98.25	this study
6H	15.64	15.27	0.37	93.50	108.77	this study
7H	16.98	20.32	-3.34	103.00	123.32	this study
8H	18.34	21.57	-3.23	112.50	134.07	this study
9H	19.95	23.23	-3.28	122.00	145.23	this study
10H	20.78	24.04	-3.26	131.50	155.54	this study
11H	21.78	25.03	-3.25	141.00	166.03	this study
12H	22.68	26.20	-3.52	150.50	176.70	this study
13H	24.57	28.17	-3.60	160.00	188.17	this study
14H	26.12	29.67	-3.55	169.50	199.17	this study
15H	27.35	30.85	-3.50	177.00	207.85	this study
16H	29.69	33.13	-3.44	186.50	219.63	this study
17H*	29.69	29.21	0.48	196.00	225.21	this study
18H*	31.11	30.63	0.48	197.20	227.83	this study
19H	32.60	32.60	0.00	201.00	233.60	ship
20H	33.71	33.71	0.00	204.90	238.61	ship
21H	35.92	35.92	0.00	214.40	250.32	ship
22H	38.33	38.33	0.00	223.90	262.23	ship
23H	40.47	40.47	0.00	233.40	273.87	ship

24H	42.29	42.29	0.00	242.90	285.19	ship
25H	42.95	43.03	-0.08	252.40	295.43	W07
26X	44.12	44.20	-0.08	261.90	306.10	W07
27X	47.38	49.28	-1.90	271.10	320.38	W07
28X	50.83	50.58	0.25	280.70	331.28	W07
29X	52.56	52.16	0.40	290.30	342.46	W07
30X	54.30	53.90	0.40	300.00	353.90	W07
31X	56.03	55.63	0.40	309.60	365.23	W07
32X	57.76	57.36	0.40	319.20	376.56	W07
33X	59.51	59.11	0.40	328.90	388.01	W07

208-1263C-

1H	13.11	12.72	0.39	90.00	102.72	this study
2H	14.98	17.5	-2.52	99.50	117.00	this study
3H	18.26	21.48	-3.22	109.00	130.48	this study
4H*	32.32	31.84	0.48	193.00	224.84	this study
5H	33.00	33.00	0.00	202.50	235.50	ship
6H	33.83	33.83	0.00	212.00	245.83	ship
7H	34.27	34.27	0.00	221.50	255.77	ship
8H	36.94	36.94	0.00	225.40	262.34	ship
9H	39.79	39.79	0.00	234.90	274.69	ship
10H	41.88	41.88	0.00	244.40	286.28	ship
11H	43.71	43.79	-0.08	253.90	297.69	W07
12H	45.42	45.5	-0.08	263.40	308.90	W07
13H	47.21	47.98	-0.77	272.90	320.88	W07
14H	50.31	49.91	0.40	282.40	332.31	W07
15H	50.31	49.91	0.40	285.60	335.51	W07
16X	50.83	51.08	-0.25	285.70	336.78	W07

208-1263D-

1H	46.48	45.76	0.72	272.00	317.76	W07
2H	48.38	47.73	0.65	275.20	322.93	W07
3H	50.61	50.34	0.27	281.50	331.84	W07
4H	50.63	50.30	0.33	284.30	334.60	W07

\* strong core disturbance

**Table S8** List of tie points to create the revised composite depth scale (rmed) for Site 1263

Hole, core, section interval (cm)	Depth			Hole, core, section interval (cm)	Depth		Source
	(mbsf)	(rmed)			(mbsf)	(rmed)	
1263A-1H-2, 50	2.00	2.00	Append to	1263A-2H-1, 0	2.30	2.71	ship
1263A-2H-7, 30	11.60	12.01	Append to	1263A-3H-1, 0	11.80	13.92	ship
1263A-3H-7, 30	21.10	23.22	Append to	1263A-4H-1, 0	21.30	25.13	ship
1263A-4H-7, 35	30.65	34.48	Tie to	1263A-6H-1, 0	40.30	47.55	ship
1263A-6H-5, 12.5	46.425	53.675	Tie to	1263B-1H-1, 37.5	46.375	53.675	this study
1263B-1H-6, 57.5	54.075	61.385	Tie to	1263A-7H-2, 102.5	52.325	61.385	this study
1263A-7H-5, 47.5	56.275	65.345	Tie to	1263B-2H-1, 85	56.35	65.345	this study
1263B-2H-5, 52.5	62.025	71.035	Tie to	1263A-8H-2, 12.5	60.925	71.035	this study
1263A-8H-6, 42.5	67.225	77.345	Tie to	1263B-3H-2, 40	66.90	77.345	this study
1263B-3H-5, 47.5	71.475	81.935	Tie to	1263A-9H-2, 50	70.80	81.935	this study
1263A-9H-7, 7.5	77.375	88.525	Tie to	1263B-4H-2, 110	77.10	88.525	this study
1263B-4H-6, 45	82.45	93.89	Tie to	1263A-10H-3, 130	82.60	93.89	this study
1263A-10H-7, 42.5	87.725	99.025	Tie to	1263B-5H-1, 77.5	84.775	99.025	this study
1263B-5H-7, 17.5	92.705	106.965	Tie to	1263C-1H-3, 125	94.25	106.965	this study
1263C-1H-6, 12.5	97.625	110.37	Tie to	1263B-6H-2, 10	95.10	110.37	this study
1263B-6H-6, 127.5	102.275	117.545	Tie to	1263C-2H-1, 55	100.05	117.545	this study
1263C-2H-7, 6	108.06	125.54	Tie to	1263B-7H-2, 72	105.22	125.54	this study
1263B-7H-6, 137.5	111.875	132.075	Tie to	1263C-3H-2, 10	110.60	132.075	this study
1263C-3H-4, 47.5	113.975	135.465	Tie to	1263B-8H-1, 140	113.90	135.465	this study
1263B-8H-4, 55	117.55	139.13	Tie to	1263A-14H-2, 30	118.10	139.13	this study
1263A-14H-6, 150	123.89	144.93	Append to	1263B-9H-1, 0	122.00	145.23	this study
1263B-9H-4, 115	127.65	150.88	Tie to	1263A-15H-1, 135	127.15	150.88	this study
1263A-15H-5, 40	132.20	155.94	Tie to	1263B-10H-1, 40	131.90	155.94	this study
1263B-10H-5, 30	137.80	161.85	Tie to	1263A-16H-1, 142.5	136.725	161.85	this study
1263A-16H-6, 17.5	142.975	168.105	Tie to	1263B-11H-2, 57.5	143.075	168.105	this study
1263B-11H-6, 75	149.25	174.29	Tie to	1263A-17H-3, 15	147.95	174.29	this study
1263A-17H-6, 15	152.45	178.80	Tie to	1263B-12H-2, 60	152.60	178.80	this study
1263B-12H-6, 80	157.50	183.71	Tie to	1263A-18H-2, 47.5	156.275	183.71	this study
1263A-18H-5, 102.5	161.325	188.765	Tie to	1263B-13H-1, 60	160.60	188.765	this study
1263B-13H-4, 132.5	165.825	194.005	Tie to	1263A-19H-1, 115	164.95	194.005	this study
1263A-19H-5, 102.5	170.825	199.895	Tie to	1263B-14H-1, 72.5	170.225	199.895	this study
1263B-14H-5, 137.5	176.875	206.555	Tie to	1263A-20H-2, 40	175.20	206.555	this study
1263A-20H-5, 70	180.00	211.37	Tie to	1263B-15H-3, 52.5	180.525	211.37	this study
1263B-15H-7, 5	186.05	216.90	Tie to	1263A-21H-1, 27.5	183.075	216.90	this study
1263A-21H-3, 97.5	186.775	220.605	Tie to	1263B-16H-1, 97.5	187.475	220.605	this study
1263B-16H-7, 57.5	196.075	229.215	<b>strong coring disturbance from 229.22 to 233.60</b>				
				1263B-19H-1	201.00	233.60	W07
1263B-19H-3, 8	204.08	236.68	Tie to	1263A-23H-2, 83.5	204.13	236.68	W07
1263A-23H-4, 48	206.76	239.31	Tie to	1263B-20H-1, 70	205.60	239.31	W07
1263B-20H-7, 33	214.22	247.93	Tie to	1263A-24H-4, 67.5	213.28	247.93	W07
1263A-24H-7, 25	217.25	251.90	Tie to	1263B-21H-2, 7.5	215.98	251.90	W07
1263B-21H-5, 103	221.42	257.34	Tie to	1263C-7H-2, 11	223.07	257.34	W07
1263C-7H-4, 15	225.28	259.55	Tie to	1263A-26H-1, 10	222.70	259.55	W07
1263A-26H-3, 120	226.80	263.65	Tie to	1263B-22H-1, 142	225.32	263.65	W07
1263B-22H-7, 65	233.55	271.88	Append to	1263A-27H-1, 0	232.10	272.13	W07
1263A-27H-6, 55	240.15	280.18	Tie to	1263C-9H-4, 98.5	240.39	280.18	W07
1263C-9H-7, 65	244.55	284.34	Tie to	1263A-28H-1, 22.5	241.82	284.34	W07
1263A-28H-3, 78	245.38	287.90	Tie to	1263B-24H-2, 121	245.61	287.90	W07
1263B-24H-6, 20	250.60	292.89	Tie to	1263C-10H-5, 61	251.01	292.89	W07
1263C-10H-7, 122	254.12	296.00	Tie to	1263A-29H-1, 112	252.22	296.00	W07
1263A-29H-5, 120	258.30	302.00	Tie to	1263C-11H-3, 138.5	258.29	302.08	W07
1263C-11H-7, 5	263.35	307.06	Tie to	1263A-30H-1, 75	261.35	307.14	W07
1263A-30H-7, 33	269.92	315.63	Tie to	1263C-12H-5, 81	270.21	315.71	W07
1263C-12H-CC, 28	273.09	318.59	Tie to	1263D-1H-1, 82.5	272.825	318.585	W07
1263D-1H-2, 115	274.65	320.41	Tie to	1263B-27X-1, 3	271.13	320.41	W07
1263B-27X-1, 145	272.55	321.83	Tie to	1263A-32H-1, 115	272.75	321.83	W07
1263A-32H-5, 30	277.90	326.98	Tie to	1263C-13H-5, 10	279.00	326.98	W07
1263C-13H-cc, 10	282.87	330.77	Append to	1263D-3H-1, 0.0	281.50	331.84	R07
1263D-3H-1, 90	282.40	332.74	Tie to	1263C-14H-1, 43	282.83	332.74	R07
1263C-14H-2, 149	285.39	335.30	Tie to	1263D-4H-1, 70	285.00	335.30	R07
1263D-4H-1, 90	285.20	335.50	Tie to	1263A-34X-1, 54	284.64	335.50	R07
1263A-34X-2, 146	287.06	337.92	Tie to	1263C-16X-1, 114	286.84	337.92	R07
1263C-16X-3, 60	288.80	339.88	end of splice				

**Table S9** Paleomagnetic data interpretation from ODP 1263

Site	Hole	Core Type	Section	Section depth (cm)	Depth mbsf	Depth rmed	Inclination (°)	Declination (°)	MAD (°)	steps used
1263	A	15H	4	91	131.21	154.94	61.9	245.7	3.3	2,3,4,5,6,7,8
1263	B	10H	1	40	131.90	155.94	42.4	159.5	5.9	2,3,4,5,6,7,8
1263	B	10H	1	140	132.90	156.94	52.1	75.2	3.8	2,3,4,5,6,7
1263	B	10H	2	90	133.90	157.94	3.8	11.3	7.1	2,3,4,5,6
1263	B	10H	3	40	134.90	158.94	48.1	32.9	5.0	2,3,4,5,6,7,8
1263	B	10H	3	140	135.90	159.94	80.2	93.3	3.3	2,3,4,5,6
1263	B	10H	4	10	136.10	160.14	56.3	307.5	2.5	2,3,4,5,6,7
1263	B	10H	4	30	136.30	160.34	65.3	43.6	4.2	2,3,4,5,6,7
1263	B	10H	4	50	136.50	160.54	-48.7	279.4	8.4	2,3,4,5,6
1263	B	10H	4	70	136.70	160.74	-64.0	224.3	4.0	2,3,4,5,6,7,8
1263	B	10H	4	90	136.90	160.94	-80.8	272.7	5.2	2,3,4,5,6,7
1263	B	10H	5	40	137.90	161.94	-49.3	223.9	4.9	2,3,4,5,6,7,8
1263	A	16H	2	101	137.81	162.94	-42.4	112.1	5.4	2,3,4,5,6,7,8
1263	A	16H	3	51	138.81	163.94	-37.0	170.3	2.6	2,3,4,5,6,7,8
1263	A	16H	4	1	139.81	164.94	-9.8	160.5	3.1	2,3,4,5,6,7,8
1263	A	16H	4	101	140.81	165.94	-20.8	114.9	5.5	2,3,4,5,6
1263	A	16H	5	51	141.81	166.94	-45.0	155.8	3.0	2,3,4,5,6,7,8
1263	A	16H	6	1	142.81	167.94	-29.2	159.8	2.0	2,3,4,5,6,7,8
1263	B	11H	2	141	143.91	168.94	-20.7	245.0	3.7	2,3,4,5,6
1263	B	11H	3	91	144.91	169.94	-24.4	247.1	4.0	2,3,4,5,6,7
1263	B	11H	4	41	145.91	170.94	-35.8	212.7	1.7	2,3,4,5,6,7,8
1263	B	11H	4	141	146.91	171.94	-46.2	161.1	5.0	3,4,5,6,7,8
1263	B	11H	5	11	147.11	172.14	37.0	189.3	5.8	2,3,4,5,6
1263	B	11H	5	31	147.31	172.34	27.5	259.2	4.7	3,4,5,6
1263	B	11H	5	51	147.51	172.54	66.6	269.7	4.2	2,3,4,5,6,7
1263	B	11H	5	71	147.71	172.74	-4.7	213.8	5.6	2,3,4,5,6,7
1263	B	11H	5	91	147.91	172.94	71.0	134.7	2.1	3,4,5,6,7
1263	B	11H	6	41	148.91	173.94	54.2	117.2	7.2	2,3,4,5,6
1263	A	17H	3	80	148.60	174.94	-56.9	3.2	6.7	2,3,4
1263	A	17H	4	30	149.60	175.94	64.8	341.3	3.4	2,3,4,5,6
1263	A	17H	4	130	150.60	176.94	70.8	312.5	3.5	2,3,4,5,6,7,8
1263	A	17H	5	80	151.60	177.94	16.3	315.3	5.0	2,3,4,5,6
1263	B	12H	2	74	152.74	178.94	-14.7	296.4	5.1	4,5,6,7
1263	B	12H	3	24	153.74	179.94	45.8	23.4	6.6	2,3,4,5,6
1263	B	12H	4	39	154.74	180.94	14.3	313.8	3.7	2,3,4,5,6,7,8
1263	B	12H	5	54	155.74	181.94	-9.3	53.9	1.6	4,5,6,7,8
1263	B	12H	6	4	156.74	182.94	12.8	295.3	1.5	2,3,4,5,6,7,8
1263	A	18H	2	70	180.44	183.94	86.5	228.4	4.4	2,3,4,5,6,7,8
1263	A	18H	3	20	181.44	184.94	79.6	140.7	3.5	2,3,4,5,6,7,8
1263	A	18H	3	120	182.44	185.94	53.2	145.5	2.5	2,3,4,5,6,7,8
1263	A	18H	4	70	183.44	186.94	73.0	51.2	3.7	2,3,4,5,6,7,8
1263	A	18H	5	20	184.44	187.94	72.8	122.2	2.4	2,3,4,5,6,7,8
1263	B	13H	1	77	160.77	188.94	82.6	339.8	2.3	2,3,4,5,6,7,8
1263	B	13H	2	27	161.77	189.94	62.9	131.6	2.6	2,3,4,5,6,7,8
1263	B	13H	2	127	162.77	190.94	44.0	147.8	5.5	2,3,4,5,6,7,8
1263	B	13H	3	77	163.77	191.94	47.8	121.9	2.3	2,3,4,5,6,7,8
1263	B	13H	4	27	164.77	192.94	49.2	146.5	5.5	3,4,5,6,7,8
1263	B	13H	4	127	165.77	193.94	69.4	253.3	6.6	2,3,4,5,6,7,8
1263	A	19H	2	58	165.88	194.94	29.7	225.4	4.3	2,3,4,5,6,7,8
1263	A	19H	3	8	166.88	195.94	53.4	296.0	3.7	2,3,4,5,6,7,8
1263	A	19H	3	108	167.88	196.94	49.1	141.1	4.8	3,4,5,6,7,8
1263	A	19H	4	58	168.88	197.94	28.1	159.4	4.1	2,3,4,5,6,7,8
1263	A	19H	5	8	169.88	198.94	47.5	321.9	4.6	2,3,4,5,6,7,8
1263	A	19H	5	108	170.88	199.94	35.4	355.1	3.8	2,3,4,5,6,7,8
1263	B	14H	1	77	170.27	199.94	39.6	305.4	3.8	2,3,4,5,6,7,8
1263	B	14H	1	97	170.47	200.14	-43.5	259.1	6.0	2,3,4,5,6,7,8
1263	B	14H	1	117	170.67	200.34	-22.4	238.1	8.9	3,4,5,6
1263	B	14H	1	137	170.87	200.54	-9.4	279.2	5.3	4,5,6
1263	B	14H	2	7	171.02	200.74	-29.7	259.5	5.4	2,3,4,5,6
1263	B	14H	2	27	171.26	200.94	-28.6	249.0	8.1	4,5,6
1263	B	14H	2	47	171.47	201.14	-82.1	270.8	1.5	2,3,4,5,6
1263	B	14H	2	127	172.27	201.94	-67.0	300.2	5.1	3,4,5,6,7,8
1263	B	14H	3	77	173.27	202.94	23.8	305.1	6.3	2,3,4,5,6,7,8
1263	B	14H	4	27	174.27	203.94	-57.7	301.9	3.5	2,3,4,5,6
1263	B	14H	4	127	175.27	204.94	-32.9	344.6	5.9	4,5,6,7,8
1263	B	14H	5	77	176.27	205.94	-74.0	315.8	3.4	4,5,6,7,8
1263	A	20H	2	78	175.58	206.94	-18.0	238.8	1.8	2,3,4,5,6,7,8

1263	A	20H	3	28	176.58	207.94	10.3	212.4	7.4	2,3,4,5,6
1263	A	20H	3	128	177.58	208.94	-0.4	256.3	2.4	4,5,6,7
1263	A	20H	4	78	178.58	209.94	8.7	238.2	2.4	2,3,4,5,6,7,8
1263	B	15H	3	20	180.20	211.05	-40.4	143.9	2.7	2,3,4,5,6,7,8
1263	B	15H	3	109	181.09	211.94	-8.7	124.4	2.0	2,3,4,5,6,7,8
1263	B	15H	4	59	182.09	212.94	-18.5	216.9	6.4	2,3,4,5,6,7
1263	B	15H	5	9	183.09	213.94	-15.7	147.0	3.8	2,3,4,5,6,7,8
1263	B	15H	5	109	184.09	214.94	-36.7	146.0	3.8	2,3,4,5,6,7,8
1263	B	15H	6	39	184.89	215.74	-46.0	169.5	1.1	2,3,4,5,6,7,8
1263	B	15H	6	59	185.09	215.94	-44.8	158.5	4.7	2,3,4,5,6,7,8
1263	B	15H	6	79	185.29	216.14	-36.7	158.3	2.2	2,3,4,5,6,7,8
1263	B	15H	6	99	185.49	216.34	-12.0	155.1	2.7	3,4,5,6,7
1263	B	15H	6	119	185.69	216.54	-6.9	147.6	2.1	3,4,5,6
1263	B	15H	6	139	185.89	216.74	16.5	170.6	3.6	2,3,4,5,6
1263	B	15H	7	9	186.09	216.94	5.7	169.8	1.2	4,5,6,7
1263	A	21H	1	31	183.11	216.94	11.9	260.4	2.3	2,3,4,5,6
1263	B	15H	7	29	186.29	217.14	-25.3	145.5	4.5	2,3,4,5,6
1263	B	15H	7	49	186.49	217.34	-12.7	148.6	6.1	2,3,4,5,6,7
1263	A	21H	1	131	184.11	217.94	46.6	251.3	3.1	2,3,4,5,6,7
1263	A	21H	2	81	185.11	218.94	10.0	1.0	2.7	2,3,4,5
1263	A	21H	3	31	186.11	219.94	2.5	272.8	3.1	3,4,5,6,7
1263	A	21H	3	131	187.11	220.94	70.8	203.5	4.5	2,3,4,5,6,7
1263	A	21H	4	81	188.11	221.94	52.3	37.0	2.6	3,4,5
1263	A	21H	5	31	189.11	222.94	12.0	274.6	2.1	3,4,5,6,7,8
1263	A	21H	5	131	190.11	223.94	57.3	2.8	3.8	2,3,4,5,6
1263	A	21H	6	81	191.11	224.94	63.9	87.7	9.0	2,3,4,5
1263	B	16H	5	31	192.81	225.94	32.0	15.5	8.4	2,3,4,5,6,7,8
1263	B	16H	5	131	193.81	226.94	66.1	62.1	3.1	2,3,4,5,6,7
1263	B	16H	6	15	194.15	227.28	-1.6	153.2	4.9	3,4,5,6,7
1263	B	16H	6	50	194.50	227.63	-9.2	191.4	5.5	4,5,6,7
1263	B	16H	6	81	194.81	227.94	-49.0	168.0	6.2	3,4,5
1263	B	16H	6	137	195.37	228.50	-35.2	192.0	6.8	3,4,5,6,7
1263	B	16H	7	35	195.85	228.98	3.7	0.9	9.0	3,4,5,6

**Table S10** Astronomical tuning age tie points

ODP 1263		ODP 702B	
depth	Age La2011	depth	Age La2011
(rmd)	(Ma)	(mbsf)	(Ma)
150.69	40.945968	91.69	41.621043
152.14	41.136030	94.92	41.818290
158.17	41.816454	98.23	42.083093
161.86	42.287809	103.22	42.513360
164.64	42.679338	112.04	43.344957
168.04	43.063264	115.02	43.522767
172.93	43.618246	116.70	43.619268
175.41	43.895737	121.26	43.894984
178.85	44.294868	126.92	44.293018
186.25	45.161553	133.80	44.740000
192.10	45.540000	148.20	45.540000
197.23	45.895194	154.36	45.898210
202.53	46.377953	162.16	46.381028
207.07	46.761879	168.83	46.757840
211.77	47.142004	175.94	47.225596
217.13	47.628564	181.74	47.545265
220.76	47.981547	190.89	48.082781
226.47	48.472441		

**Table S11** Comparison of magnetochron boundary ages in million years

Chron	standard GPTS			tuned			tuned – this study <sup>†</sup>		
	CK95	GPTS		PEAT Sites <sup>‡</sup>	Contessa Hyw	ODP Site 1260	ODP Site 1258 opt.2	ODP Site 1263	ODP Site 702B
		2004	2012						
C18n.2n (o)	40.130	39.464	40.145	40.076 ± 5	40.120				
C19n (y)	41.257	40.439	41.154	41.075 ± 7	41.250	41.061 ± 9		41.030 ± 13	
C19n (o)	41.521	40.671	41.390	41.306 ± 5	41.510	41.261 ± 4		41.180 ± 11	
C20n (y)	42.536	41.590	42.301	42.188 ± 15	42.540	42.152 ± 7		42.107 ± 13	42.124 ± 4
C20n (o)	43.789	42.774	43.432		43.790	43.449 ± 18		43.517 ± 11	43.426 ± 3
C21n (y)	46.264	45.346	45.724		46.310			46.151 ± 9	46.080 ± 3
C21n (o)	47.906	47.235	47.349				47.723 ± 118	47.575 ± 18	
C22n (y)	49.037	48.599	48.566				48.954 ± 16		
C22n (o)	49.714	49.427	49.344				49.593 ± 42		
C23n.1n (y)	50.778	50.730	50.628				51.051 ± 21		
C23n.1n (o)	50.946	50.932	50.835				51.273 ± 39		
C23n.2n (y)	51.047	51.057	50.961				51.344 ± 32		
C23n.2n (o)	51.743	51.901	51.833				51.721 ± 23		
C24n.1n (y)	52.364	52.648	52.620				52.525 ± 23		
C24n.1n (o)	52.663	53.004	53.074				52.915 ± 29		
C24n.2n (y)	52.757	53.116	53.199				53.037		
C24n.2n (o)	52.801	53.167	53.274				53.111		
C24n.3n (y)	52.903	53.286	53.416				53.249 ± 17		
C24n.3n (o)	53.347	53.808	53.983				53.806 ± 20		

<sup>†</sup> tuned to the orbital solution La2011 (Laskar et al. 2011)<sup>‡</sup> combined ages based on Pacific Equatorial Age Transect Sites 1218, U1333 and U1334 (Westerhold et al. 2014)**Table S12** Comparison of magnetochron boundary durations in million years

Chron	standard GPTS			tuned			tuned – this study <sup>†</sup>		
	CK95	GPTS		PEAT Sites <sup>‡</sup>	Contessa Hyw	ODP Site 1260	ODP Site 1258 opt.2	ODP Site 1263	ODP Site 702B
		2004	2012						
C18n.2r	1.127	0.975	1.009	0.999 ± 12					
C19n	0.264	0.232	0.236	0.231 ± 12	0.260	0.200 ± 7		0.150 ± 24	
C19r	1.015	0.919	0.911	0.882 ± 20	1.030	0.891 ± 6		0.927 ± 24	
C20n	1.253	1.184	1.131		1.250	1.297 ± 13		1.410 ± 24	1.302 ± 7
C20r	2.475	2.572	2.292		2.520			2.634 ± 20	2.654 ± 6
C21n	1.642	1.889	1.625					1.424 ± 27	
C21r	1.131	1.364	1.217				1.231 ± 134		
C22n	0.677	0.828	0.778				0.639 ± 58		
C22r	1.064	1.303	1.284				1.458 ± 63		
C23n.1n	0.168	0.202	0.207				0.222 ± 60		
C23n.1r	0.101	0.125	0.126				0.071 ± 71		
C23n.2n	0.696	0.844	0.872				0.377 ± 55		
C23n.2r	0.621	0.747	0.787				0.804 ± 46		
C24n.1n	0.299	0.356	0.454				0.390 ± 52		
C24n.1r	0.094	0.112	0.125				0.122		
C24n.2n	0.044	0.051	0.075				0.074		
C24n.2r	0.102	0.119	0.142				0.138		
C24n.3n	0.444	0.522	0.567				0.557 ± 37		

<sup>†</sup> tuned to the orbital solution La2011 (Laskar et al. 2011)<sup>‡</sup> combined ages based on Pacific Equatorial Age Transect Sites 1218, U1333 and U1334 (Westerhold et al. 2014)**Table S13.** Comparison of durations of magnetochrons in million years including uncertainties in magnetic anomaly width

Chron	CK95		GPTS2004		GPTS2012		this study		Source Site
	min	max	min	max	min	max	min	max	
C19	1.197	1.360	1.069	1.232	1.066	1.228	1.074	1.106	ODP 1260 <sup>*</sup>
C20n	1.172	1.334	1.103	1.266	1.050	1.212	1.273	1.323	ODP 1260 <sup>*</sup>
C20r	2.324	2.626	2.420	2.723	2.141	2.443	2.675	2.729	ODP 1260 <sup>*</sup> , 1263 <sup>‡</sup>
C21n	1.506	1.778	1.753	2.026	1.489	1.761	1.397	1.451	ODP 1263 <sup>‡</sup>
C21r	0.975	1.287	1.209	1.520	1.061	1.373	1.345	1.413	ODP 1258 <sup>§</sup>
C22n	0.615	0.739	0.765	0.890	0.716	0.840	0.581	0.697	ODP 1258 <sup>§</sup>
C22r	0.911	1.217	1.150	1.456	1.131	1.437	1.395	1.521	ODP 1258 <sup>§</sup>
C23	1.241	1.931	1.574	2.263	1.647	2.337	1.430	1.518	ODP 1258 <sup>§</sup>
C24	3.119	3.961	3.596	4.438	4.060	4.902	4.492	4.558	ODP 1258 <sup>§</sup> , 1262 <sup>**</sup>

<sup>\*</sup>Westerhold & Röhl (2013); <sup>‡</sup>this study; <sup>§</sup>Westerhold & Röhl (2009); <sup>\*\*</sup>Westerhold et al. (2007; option 2)

Note: minimum and maximum durations for CK95, GPTS2004 and GPTS2012 are based on the error given for the mean width of magnetic anomalies as published in table 4 of Cande &amp; Kent (1992)